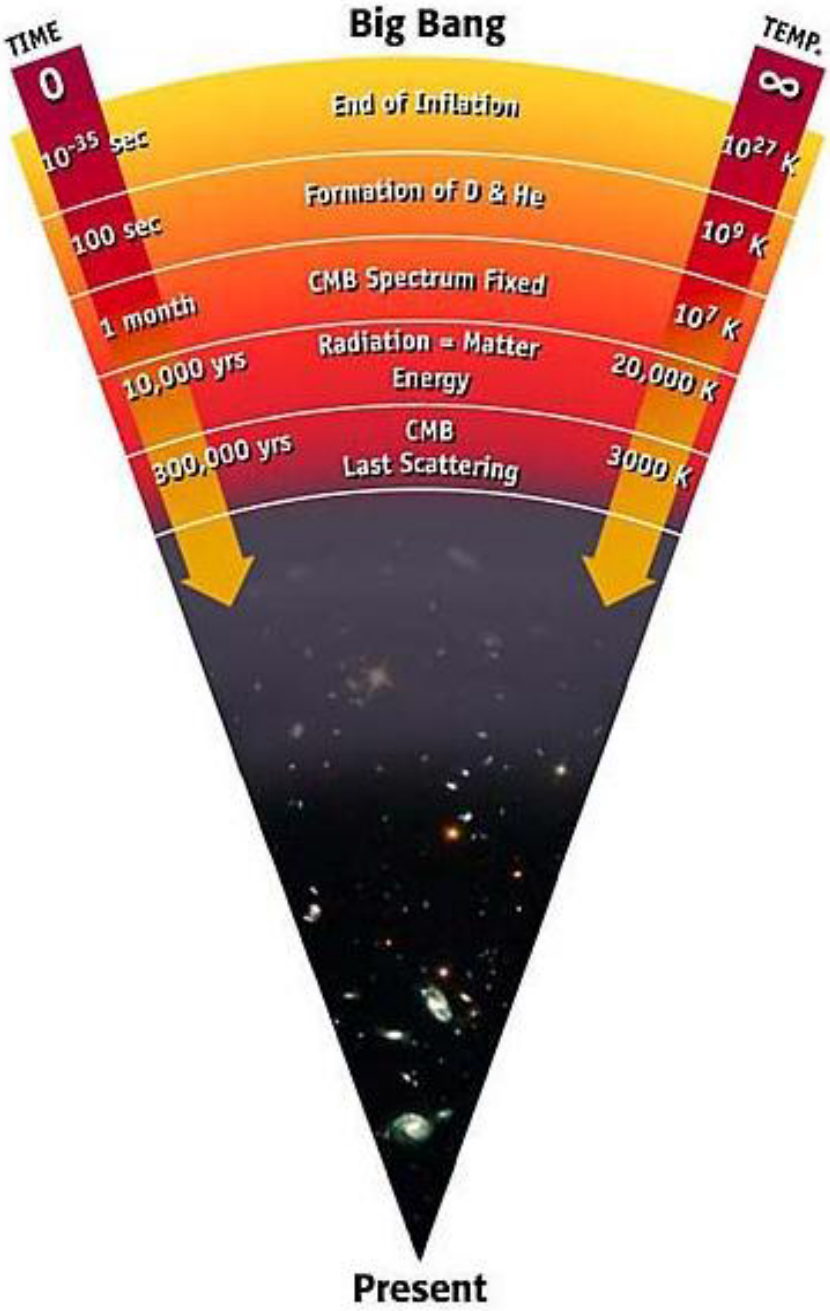

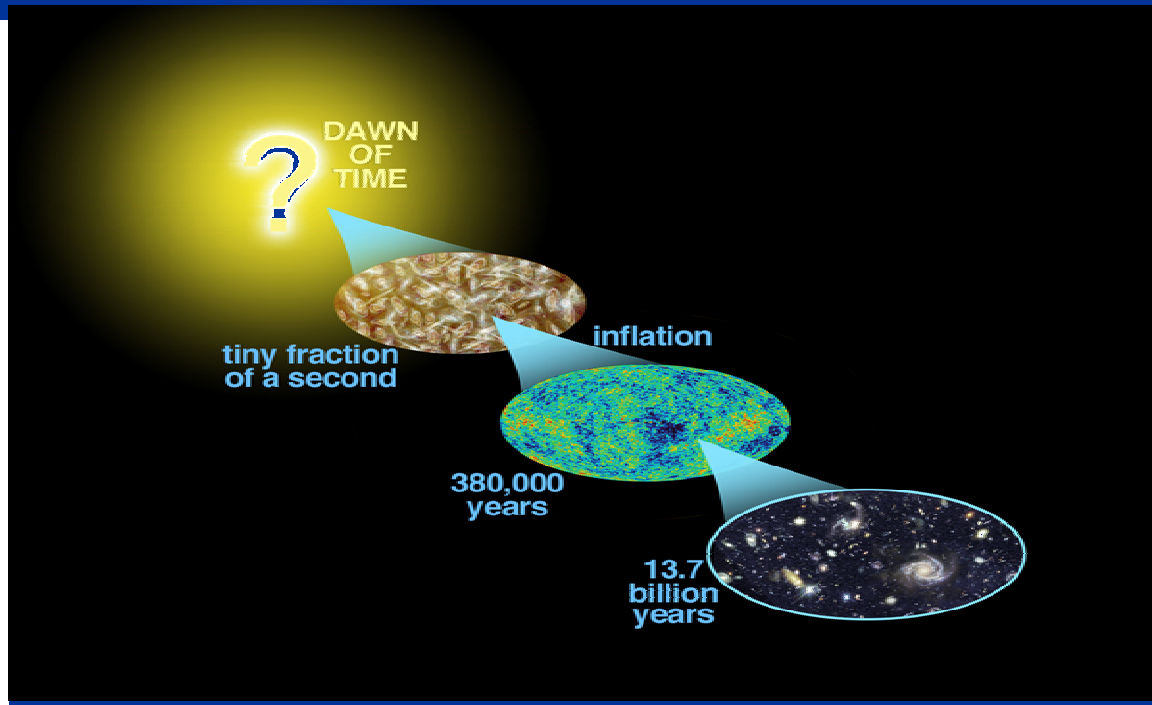

- Big Bang
- Recombination
- Dark Ages
- Formation of stars, galaxies and QSOS
- Reheating and reionization

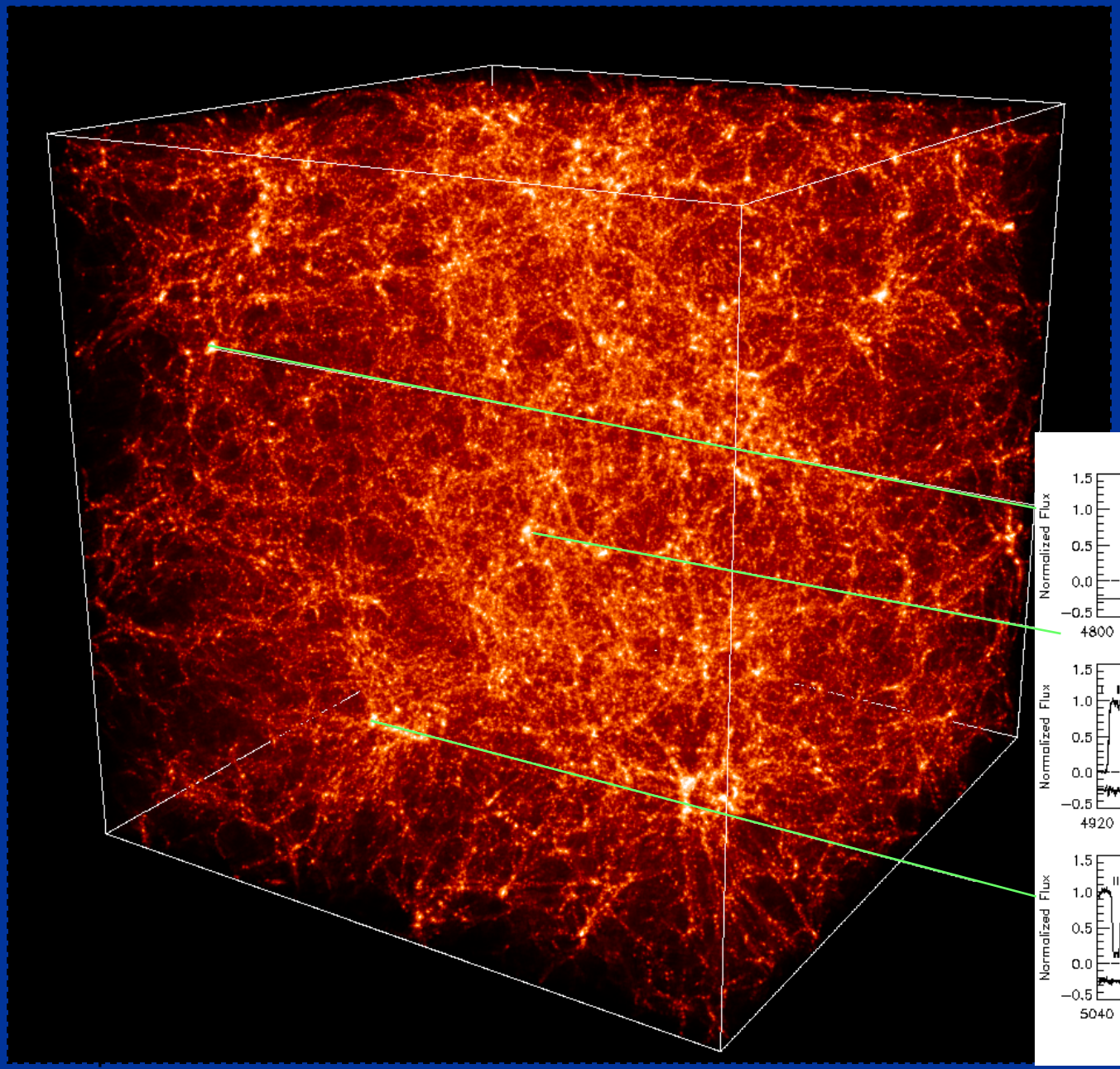

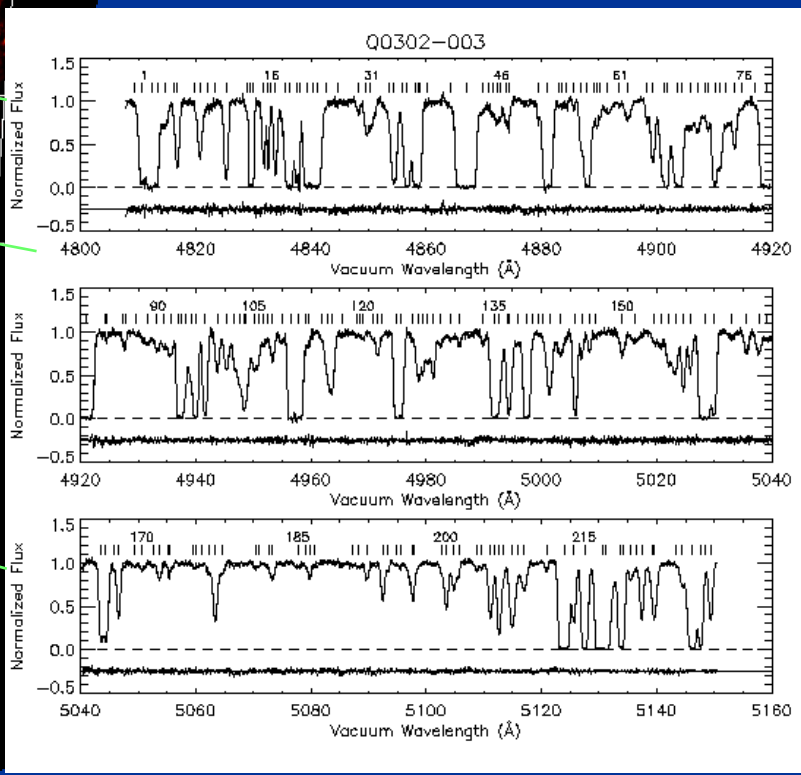
Q0302−003
Normalized Flux
Vacuum Wavelength (Å)
1.5
1.0
0.5
0.0
−0.5
4800
4820
4840
4860
4880
4900
4920
4940
4960
4980
5000
5020
5040
5060
5080
5100
5120
5140
5160

A UVES absorption spectrum

A beam of light coming from a distant quasar passes through numerous intervening gas clouds in galaxies and in intergalactic space. These clouds of primeval matter subtract specific colours from the beam. The resulting 'absorption spectrum', recorded by the VLT UV-Visual Echelle Spectrograph (UVES), is used to determine the distances, physical properties and chemical composition of the invisible clouds.

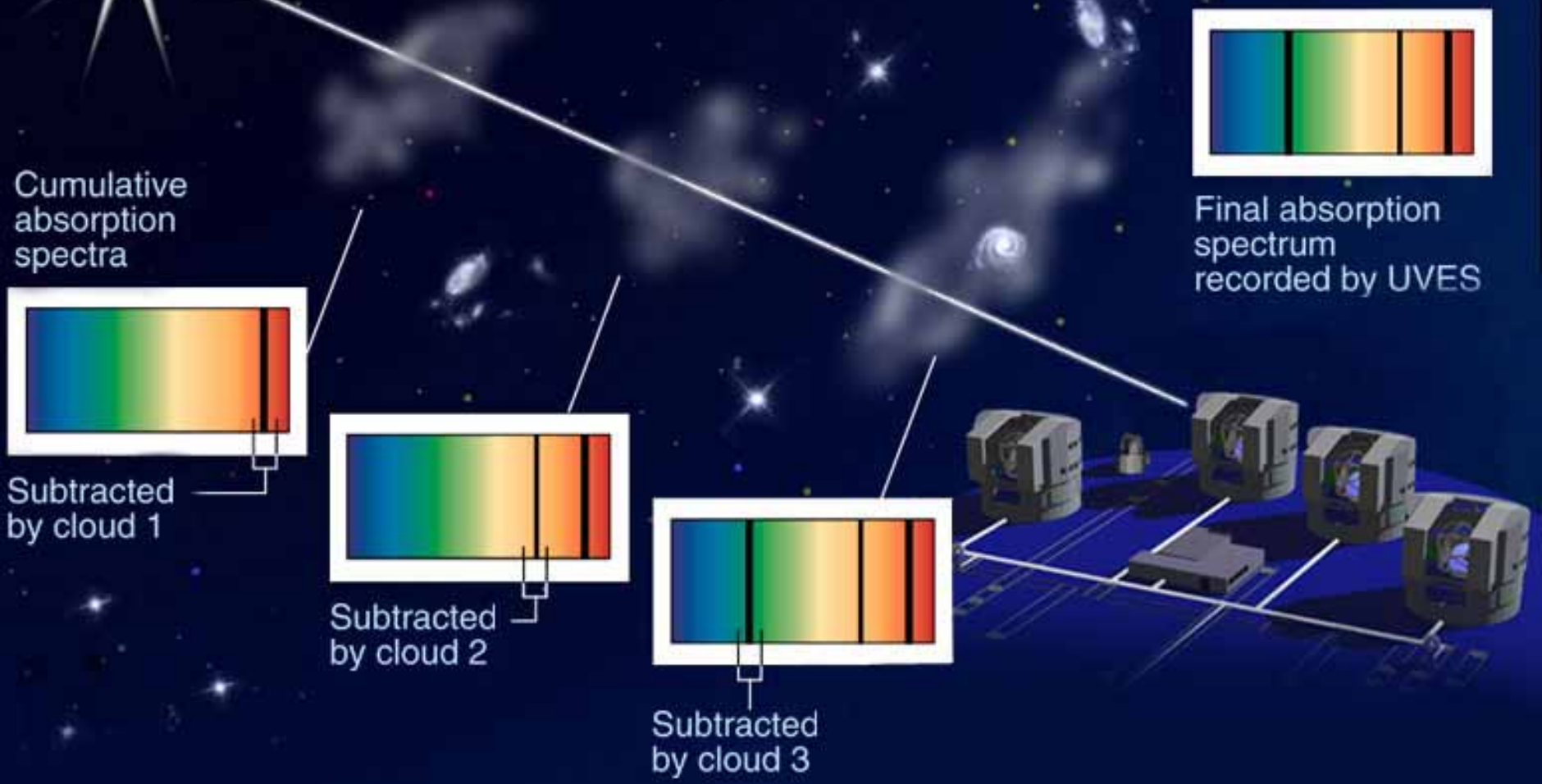

IGM - absorption lines

A unique and independent source of information between the CMB, at z~1000, and the large scale distribution of galaxies

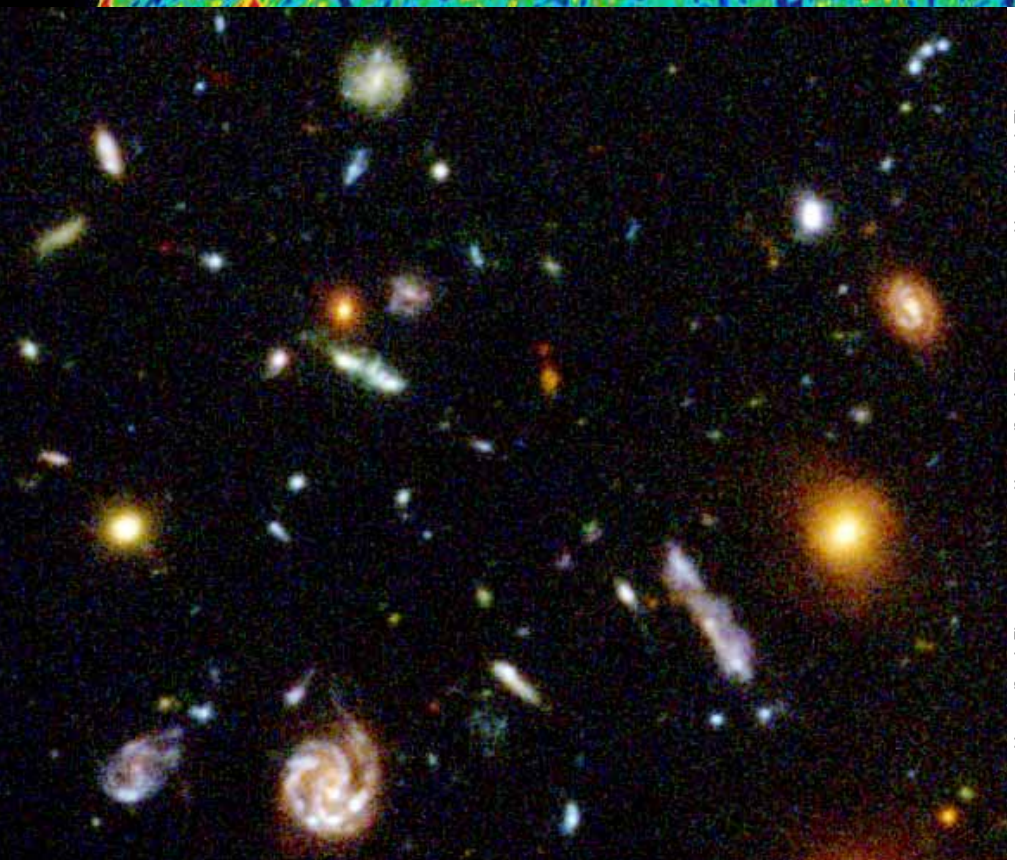

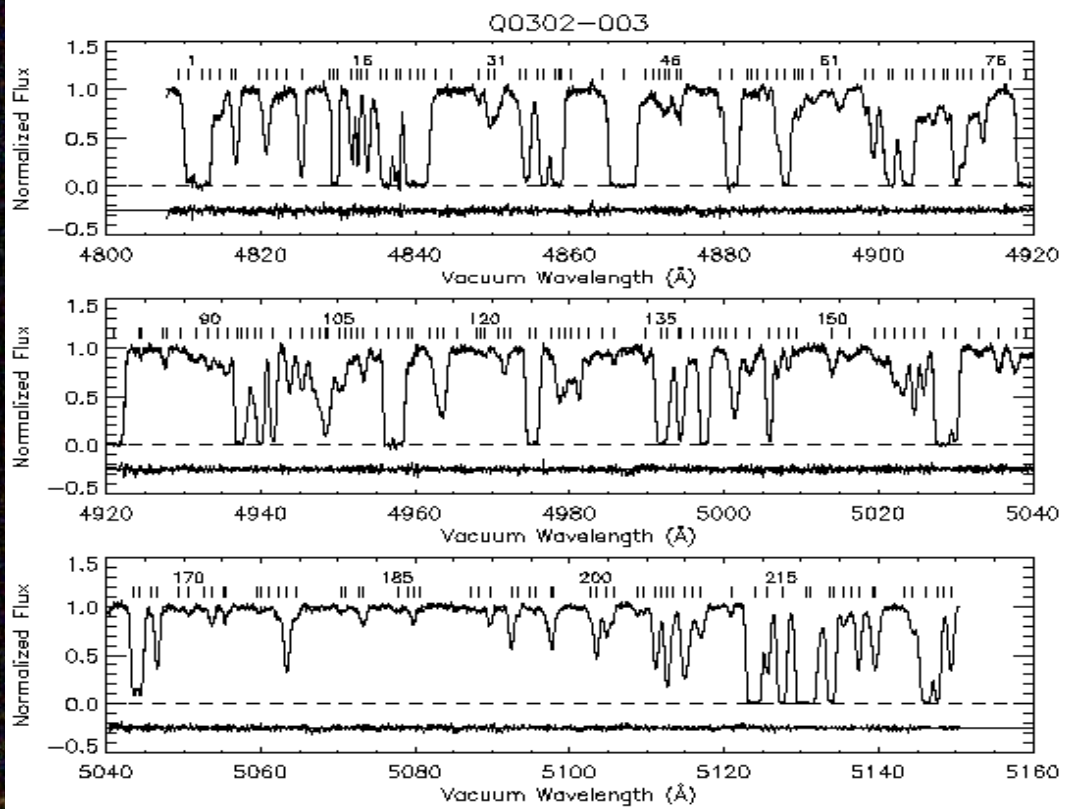

IGM - Absorption Lines - Goals

- What were the physical conditions of the primordial Universe?
- What fraction of the matter was in a diffuse medium and how early did it condense in clouds?
- Where are most of the baryons at the various redshifts?
- When and how did the formation of galaxies and LSS start?
- How early and in what amount have metals been produced?
- What was the typical radiation field, how homogenous, and what was producing it?
- When and how, after the Dark Ages following recombination, did the Universe get reionized?
- Does the SBBN correctly predict primordial element abundances and CMB evolution?
- Do fundamental constants of physics (e.g. α) vary with time?

INTERGALACTIC MEDIUM
Lecture 1

Stefano Cristiani

cristiani@ts.astro.it

http://www.oat.ts.astro.it/~cristiani/

QSO absorption Lines: a bit of history

1965, Gunn & Peterson GP test

1965, Bahcall & Salpeter

- the presence of diffuse neutral hydrogen expected to be revealed by an absorption trough bluewards of the Lyman-α emission, which had not been observed in the spectrum of the quasar 3C 9 obtained by Schmidt.

1966, Burbidge et al.: 3C191 - absorptions detected!

1971, Lynds: 4C 05.34 Lyman-α forest

The Gunn-Peterson Test (1965, ApJ 142, 1633)

NOTES

ON THE DENSITY OF NEUTRAL HYDROGEN IN INTERGALACTIC SPACE

Recent spectroscopic observations by Schmidt (1965) of the quasi-stellar source 3C 9, which is reported by him to have a redshift of 2.01, and for which Lyman-α is in the visible spectrum, make possible the determination of a new very low value for the density of neutral hydrogen in intergalactic space. It is observed that the continuum of the source continues (though perhaps somewhat weakened) to the blue of Ly-α; the line as seen on the plates has some structure but no obvious asymmetry. Consider, however, the fate of photons emitted to the blue of Ly-α. As we move away from the source along the line of sight, the source becomes redshifted to observers locally at rest in the expansion, and for one such observer, the frequency of any such photon coincides with the rest frequency of Ly-α in his frame and can be scattered by neutral hydrogen in his vicinity. The calculation of the size of the effect is very easily performed as follows:

Let us consider a cosmological model with the metric

$$ds^2 = dl^2 - R^2(t)\,(du^2 + \sigma^2(u)d\gamma^2)\,,$$

where

$$\sigma(u) = \begin{cases} \sin u\,, \\ u \\ \sinh u \end{cases}$$

depending on the curvature, and $d\gamma$ is the increment in angle.

The probability of scattering of a photon in a *proper* length interval $dl = R(t)du$ at cosmic time t is clearly

$$dp = n(t)\sigma(\nu_a)dl\,,$$

where $n(t)$ is the number of neutral hydrogen atoms per unit volume at time t (assumed uniform for the present) and $\sigma(\nu)$ is the radiative excitation cross-section for the Ly-α transition. This has the form

$$\sigma(\nu) = \frac{\pi e^2}{m c} f\, g(\nu - \nu_a)\,,$$

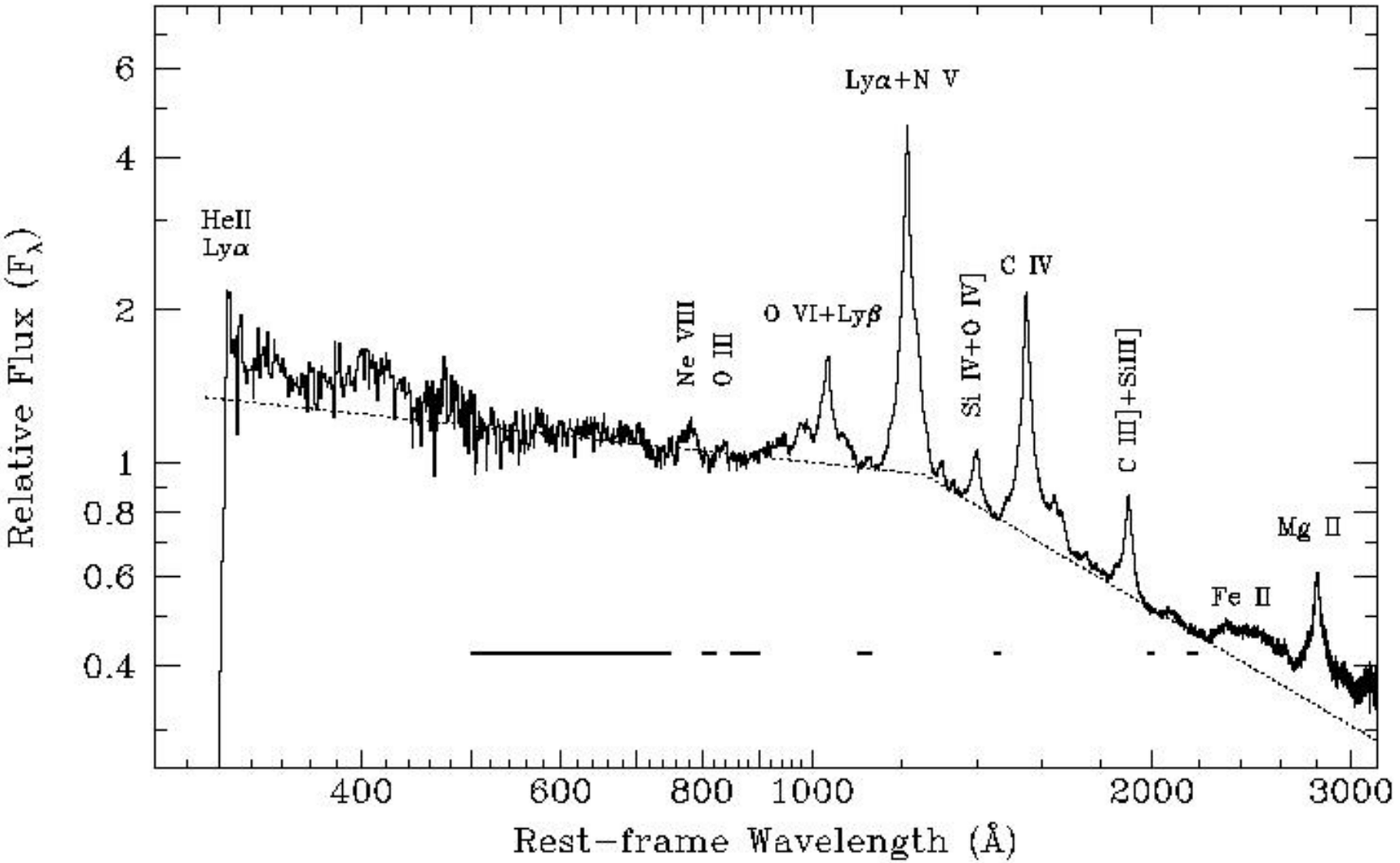

Figure 1: (Telfer et al. 2001) Overall mean composite QSO spectrum in 1 Å bins with some prominent emission lines marked.

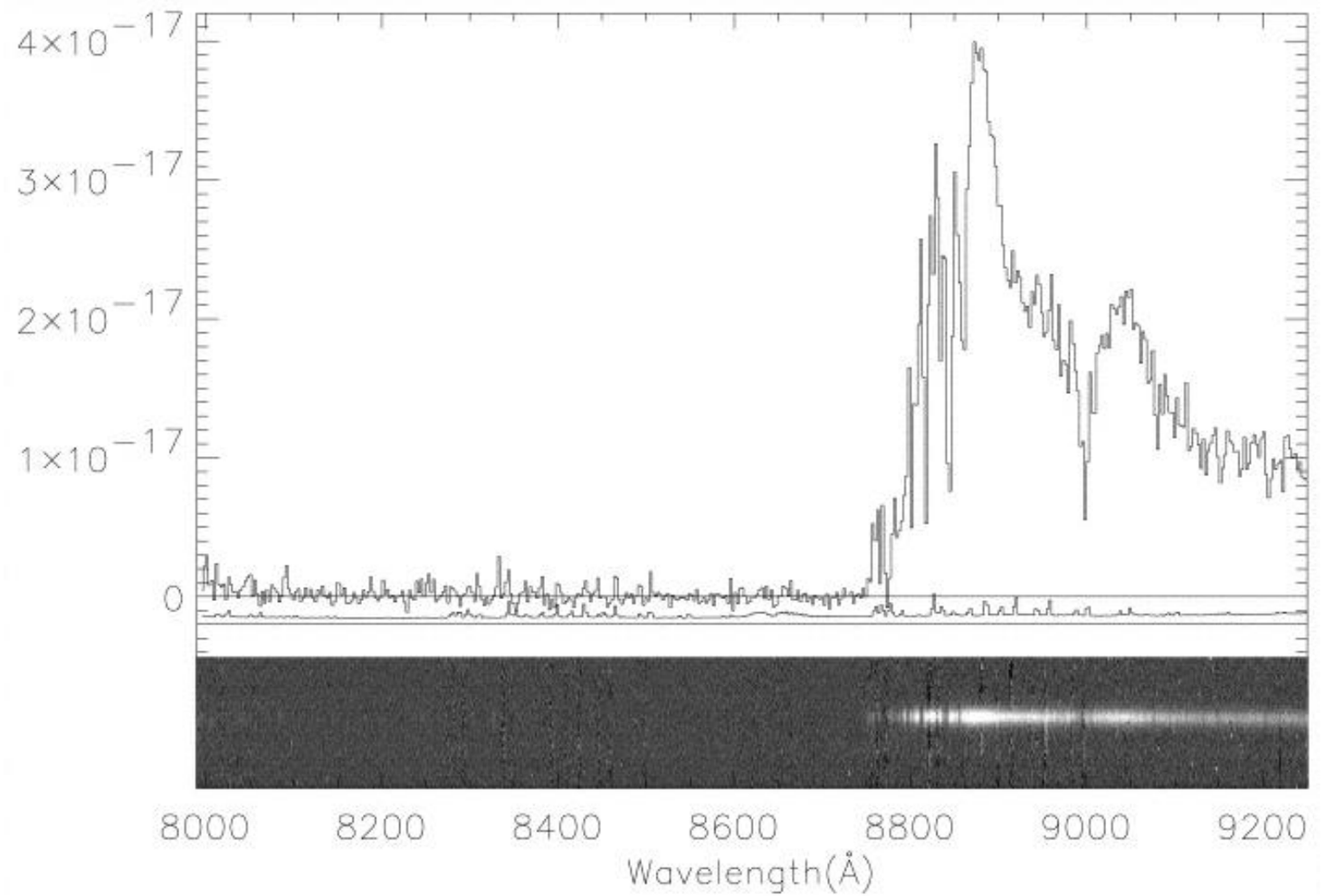

Upper panel: the VLT/FORS2 one-dimensional optical spectrum of the $z = 6.28$ quasar SDSS 1030+0524 shown in the observed frame and smoothed to a dispersion of 3 Å pixel^{-1}. The bottom line shows the error array derived from the sky spectrum and offset by -0.2×10^{-17} cgs for clarity. Lower panel: a grey-scale representation of the sky-subtracted two-dimensional spectrum plotted on the same wavelength scale. The spatial extent of the plot is 40 pixels, corresponding to 20 arcseconds. Data from Pentericci et al. 2002.

The Gunn-Peterson Test (1965, ApJ 142, 1633)

Gunn and Peterson did detect some absorption but the light of the QSO was not completely absorbed and there was some residual light left in the spectral region in question. The relative weakness of the absorption could mean two things:

a) there is little hydrogen left in intergalactic space and by the time the Lyman-α forest is observed most of the matter has already condensed into galaxies.

b) most of the hydrogen is not in neutral form, where it can produce Lyman-α absorption, but is fully ionized.

QSO absorption Lines: a bit of history

1965, Gunn & Peterson GP test

- the presence of diffuse neutral hydrogen expected to be revealed by an absorption trough bluewards of the Lyman-α emission, which had not been observed in the spectrum of the quasar 3C 9 obtained by Schmidt.

1965, Bahcall & Salpeter $\Leftarrow$

- intervening material (galaxies) should produce observable discrete absorption features in QSO spectra

1966, Burbidge et al.: 3C191 - absorptions detected!

1971, Lynds: 4C 05.34 Lyman-α forest

3C191 - absorptions detected! (Burbidge et al. 1966)

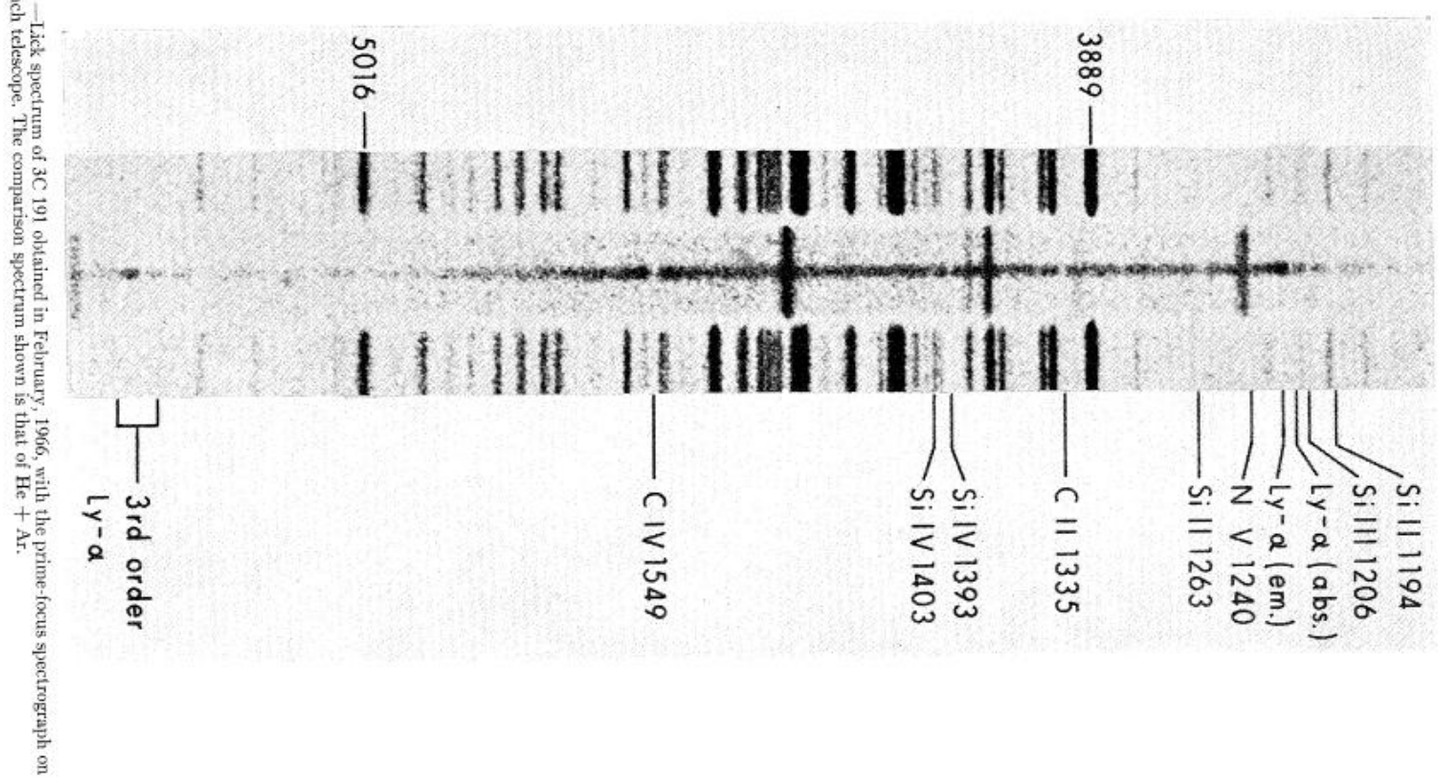

Fig. 2.—Lick spectrum of 3C 191 obtained in February, 1966, with the prime-focus spectrograph on 120-inch telescope. The comparison spectrum shown is that of He + Ar.

Lines due to gas emitted by the quasar itself or originated by intervening material?

1969: Bahcall and Spitzer: most absorption systems with metals produced by the halos of normal galaxies

The Lyman Forest: 4C 05.34 (Lynds, 1971)

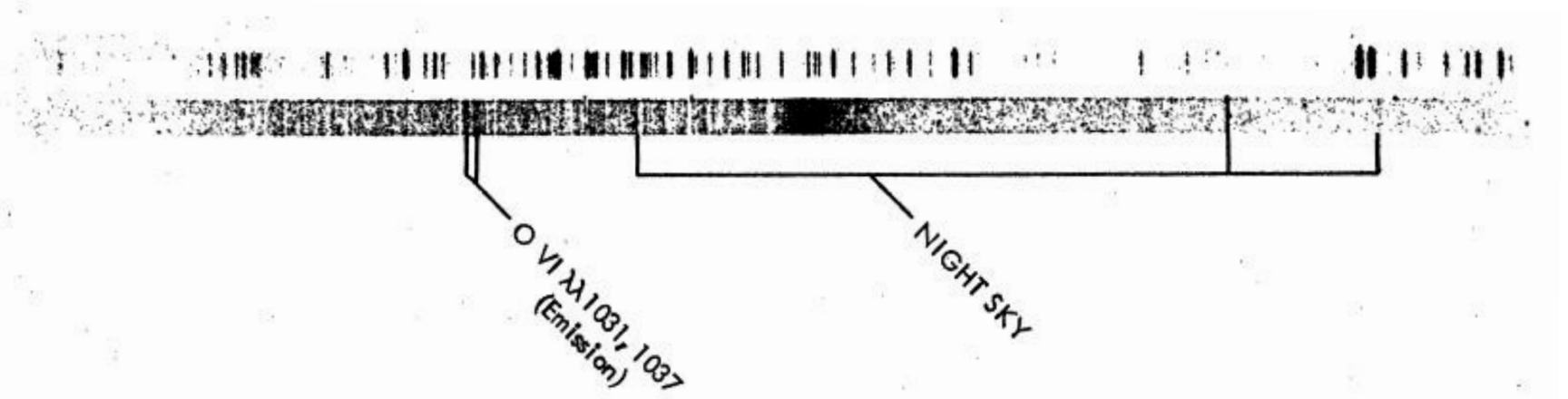

FIG. 1.—A spectrogram illustrating the numerous absorption lines in 4C 05.34. The strong emission line in the center is Lα. The O VI emission lines and several airglow features are also indicated. The comparison spectrum is He + Ar + Ne.

One of the first QSOs with $z > 2.5$. The region bluewards of the Lyman-α emission accessible to ground observations. A "*forest*" of absorption lines, much more numerous than in the region longward the Lyman-α emission.

Interpret: a large number of intervening Lyman-α absorbers.

As more data accumulated, the sheer number of Lyman-α forest lines strongly supported the idea that galactic and intergalactic gas, and not only material intrinsic to the quasar, is the source of most quasar absorption lines.

Classes of Absorbers

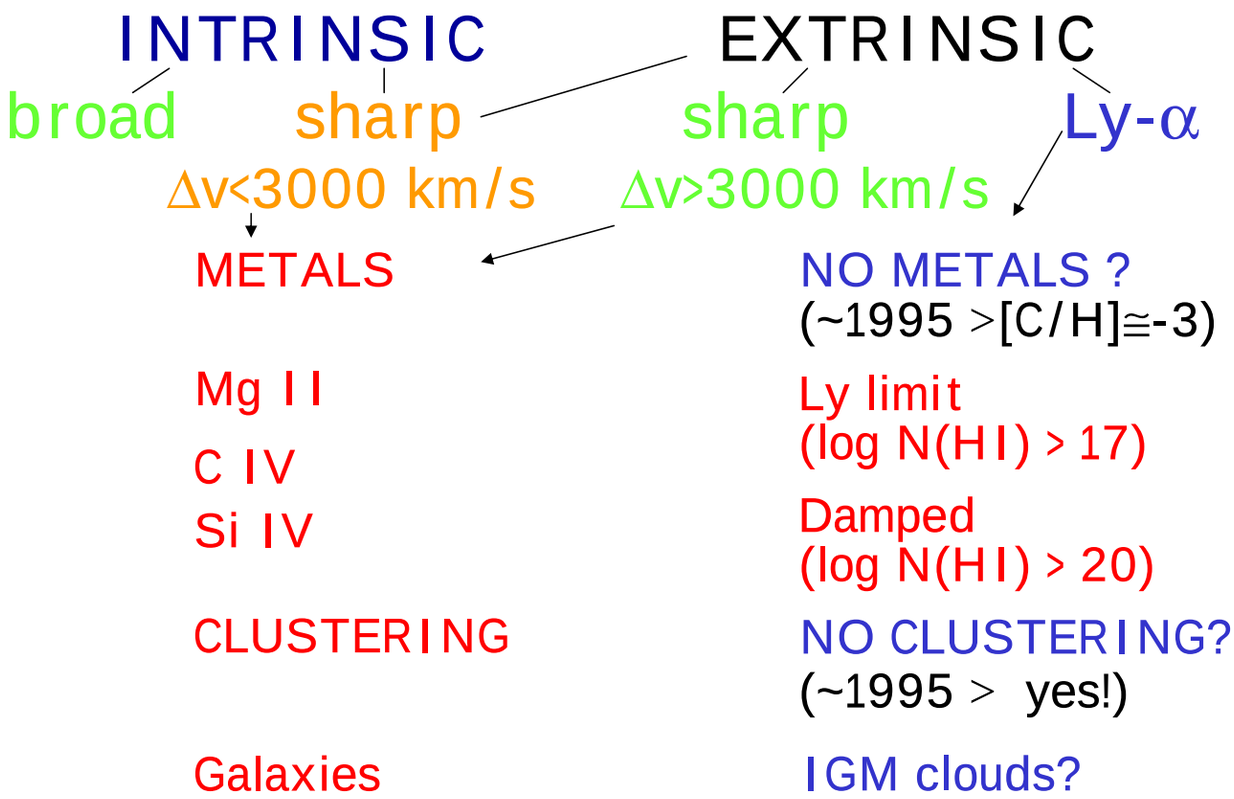

Broad Absorption Line QSOs

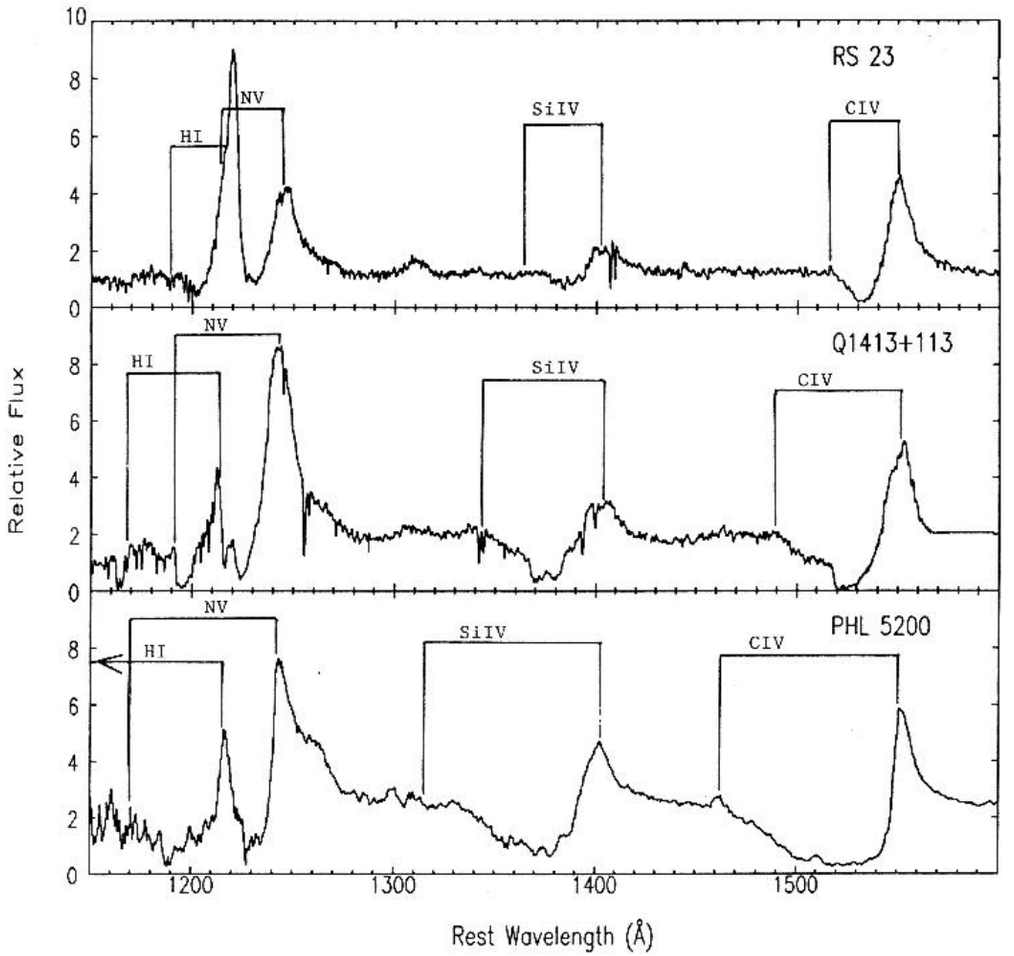

intrinsic, due to gas outflowing from the AGN, by analogy with P-Cyg profiles in stars

Broad Absorption Line QSOs - scheme

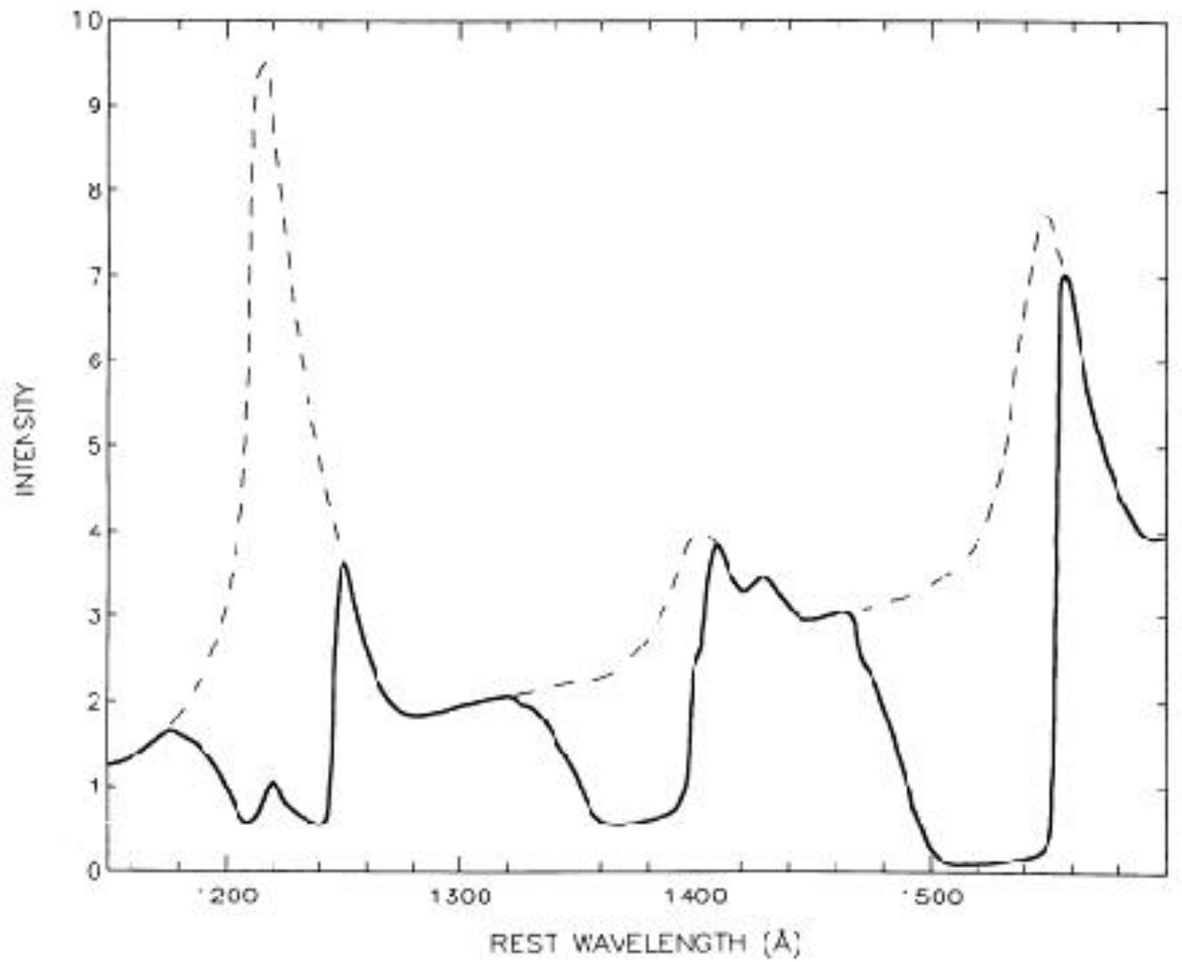

QSO absorption lines:

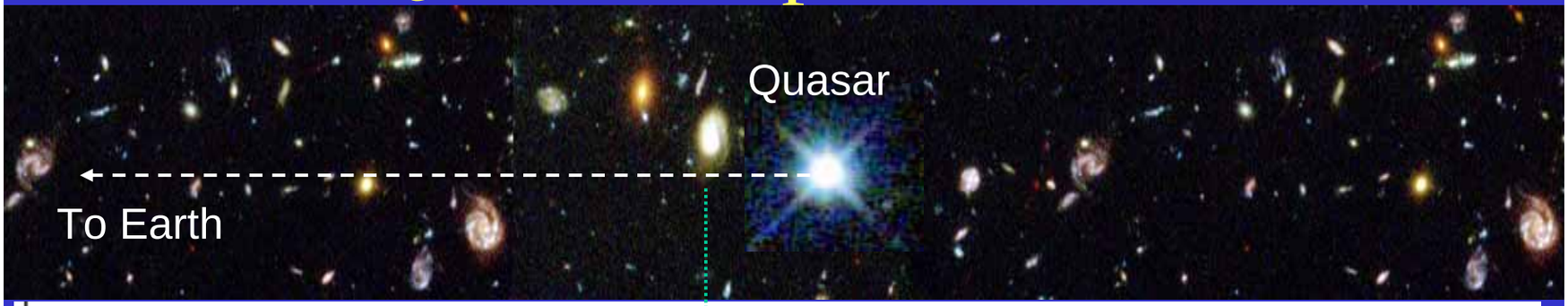

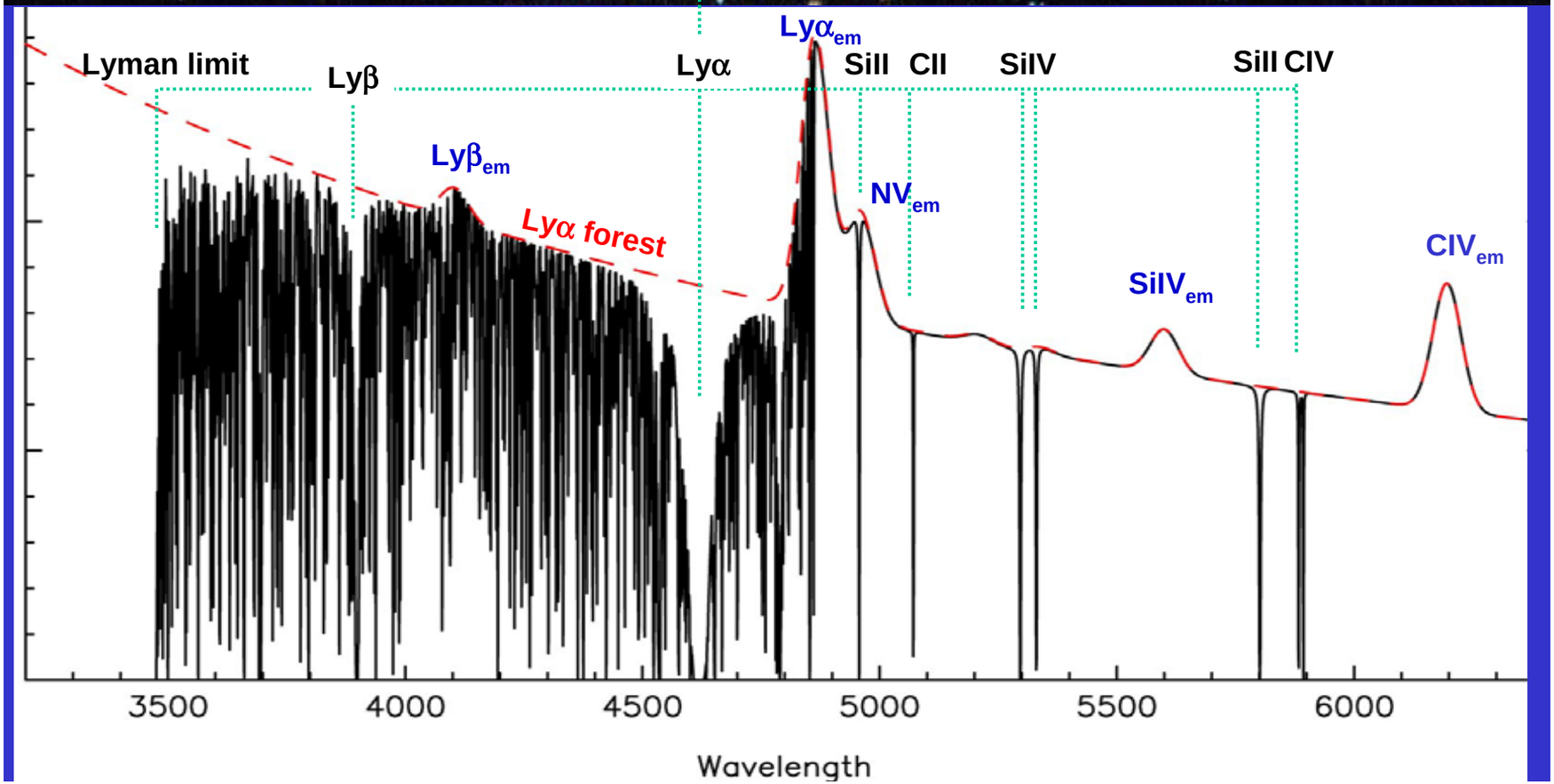

Classes of Absorbers

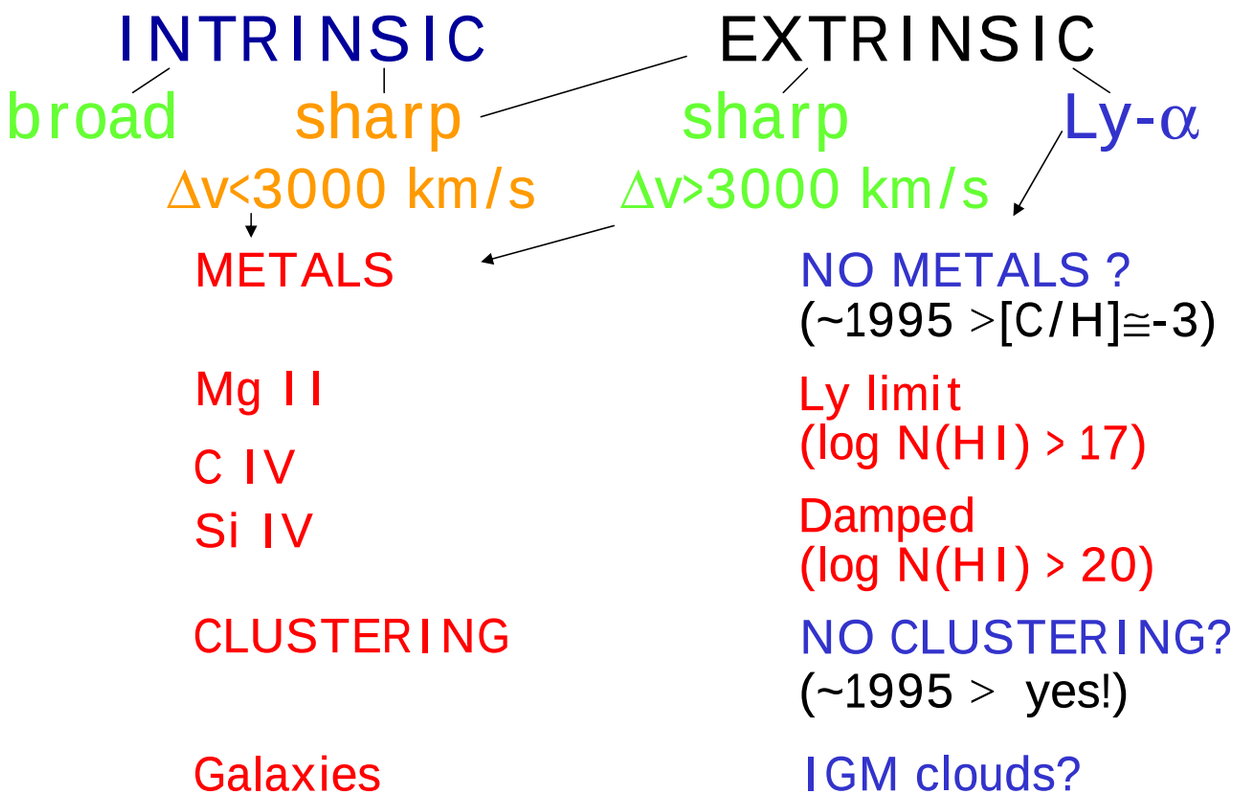

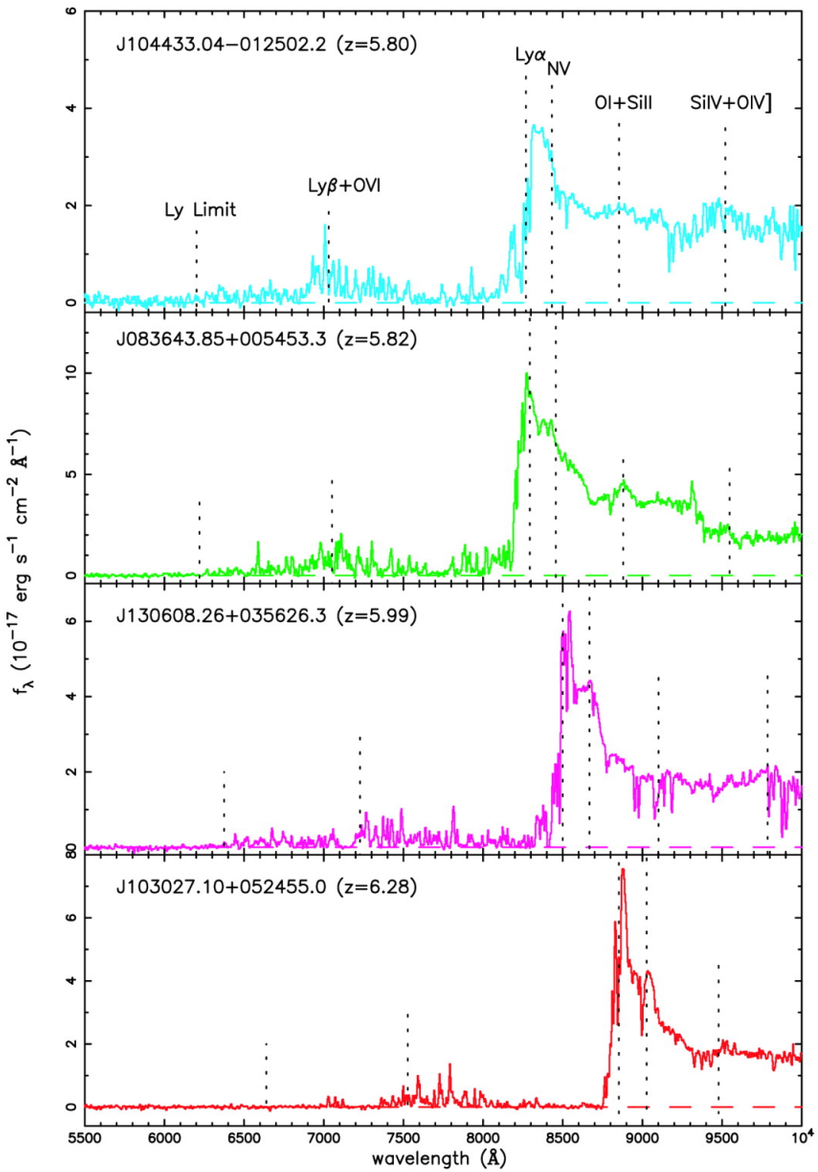

From Becker et al. AJ 122, 2850 (2001)

The Light Path $\frac{dl}{dz}$

$$dl = c\,dt = c\,\frac{da}{\dot{a}} \Rightarrow \frac{dl}{dz} = \frac{c}{\dot{a}}\,\left|\frac{da}{dz}\right|$$

$$\left|\frac{da}{dz}\right| = \left|\frac{d}{dz}\,\frac{a_o}{1+z}\right| = \frac{a_o}{(1+z)^2} = \frac{a}{1+z}$$

$$dl = c\,\frac{a}{\dot{a}(1+z)}$$

$$\frac{\dot{a}}{a} = H_o\,E(z) = H_o\,\left[\Omega\,(1+z)^3 + \Omega_R\,(1+z)^2 + \Omega_\Lambda\right]^{1/2}$$

$$\Omega = \frac{8\pi G\rho_o}{3H_o^2} \qquad \Omega_R = \frac{1}{(H_o\,a_o\,R)^2} \qquad \Omega_\Lambda = \frac{\Lambda}{3H_o^2}$$

$$\frac{dl}{dz} = \frac{c}{H_o\,(1+z)\,E(z)} \tag{1}$$

$$\Omega_\Lambda = 0,\ \Omega_R = 0 \Rightarrow \frac{dl}{dz} = \frac{c}{H_o}(1+z)^{-5/2}$$

$$\Omega = 0,\ \Omega_R = 1 \Rightarrow \frac{dl}{dz} = \frac{c}{H_o}(1+z)^{-2}$$

GUNN-PETERSON EFFECT

$$\nu_o = \frac{\nu_e}{(1+z_e)} \qquad 1+z = (1+z_e)\frac{\nu_\alpha}{\nu_e}$$

$$\Rightarrow \text{ Local } \quad \text{Lyman-}\alpha \quad \text{resonance}$$

$$\sigma(\nu) = \sigma(\nu_o \frac{a_o}{a}) = \frac{\pi e^2}{m_e c}\ f\ \Phi(\nu_o \frac{a_o}{a})$$

$$f = 0.4162 \quad \textit{oscillator strength;} \quad \Phi(\nu) \simeq \delta(\nu - \nu_{Ly-\alpha})$$

$$\tau_{GP} = \int \sigma(\nu_o \frac{a_o}{a}) n_{HI}\ dl$$

$$dl = c\ dt = c\ \frac{da}{\dot{a}}$$

$$\tau_{GP} = \int \sigma\ n_{HI}\ c\ \frac{da}{\dot{a}} = \int \frac{\sigma\ n_{HI}\ c}{H_o\ a\ E(a)} da$$

$$E(a) = [\Omega_M \, (\frac{a_o}{a})^3 + \Omega_R \, (\frac{a_o}{a})^2 + \Omega_\Lambda]^{1/2}$$

$$\tau_{GP} = \int \frac{\sigma_x \, n_{HI} \, c}{H_o \, E(x)} \, \frac{x}{\nu_o \, a_o} \, \frac{\nu_o \, a_o}{x^2} \, dx \qquad\qquad x = \frac{\nu_o \, a_o}{a}$$

$$\tau_{GP} = \frac{\pi e^2}{m_e c} \, f \, \frac{n_{HI} \, c}{H_o \, E(z) \, \nu_\alpha} = \frac{\pi e^2}{m_e \, \nu_\alpha} \, f \, \frac{n_{HI}}{H_o \, E(z)}$$

$$n_{HI} = 2.4131 \cdot 10^{-11} \, h \, \tau(z) \, E(z)$$

$$\frac{\bar{n_H}}{(1-Y) \, (1+z)^3} = \Omega_b \, \rho_o = 1.88 \cdot 10^{-29} \, \Omega_b \, h^2 \, g/cm^3 = 1.124 \cdot 10^{-5} \, \Omega_b \, h^2 \, prot/cm^3$$

$$\frac{n_{HI}}{\bar{n_H}} = \frac{2.4131 \cdot 10^{-11} \, h \, \tau(z) \, E(z)}{(1-Y) \, 1.124 \cdot 10^{-5} \, (1+z)^3 \, \Omega_b \, h^2} = \frac{1.5 \cdot 10^{-4} \, h \, \tau(z) \, E(z)}{(1+z)^3} \, (\frac{0.019}{\Omega_b \, h^2})$$

$$\tau_{GP \; EdS} = 6.6 \cdot 10^3 \, h^{-1} \, \frac{\Omega_b \, h^2}{0.019} \, \frac{n_{HI}}{\bar{n_H}} \, (1+z)^{3/2}$$

$$\tau_{GP} < 0.1 \quad @ \; z \sim 5 \quad \Rightarrow \quad \frac{n_{HI}}{\bar{n_H}} < 10^{-6} \, h$$

$$@ \; z \sim 6 \;\; \tau_{GP} \sim 5 \quad \Rightarrow \quad \frac{n_{HI}}{\bar{n_H}} \sim 4 \cdot 10^{-5} \, h \quad 99.995\% \; ionized!$$

Deriving physical quantities from absorption lines

Detailed treatment in a number of introductory texts, for example Gray (1992), Spitzer (1978), and Swihart(1976).

Voigt profile fits

The profiles of real spectral lines are not infinitely narrow.

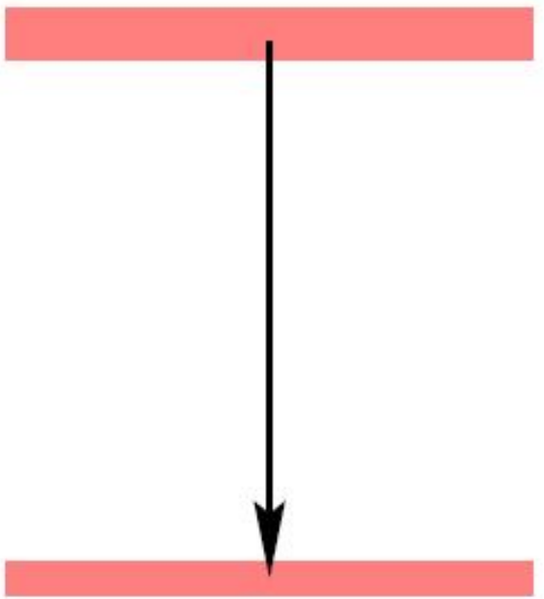

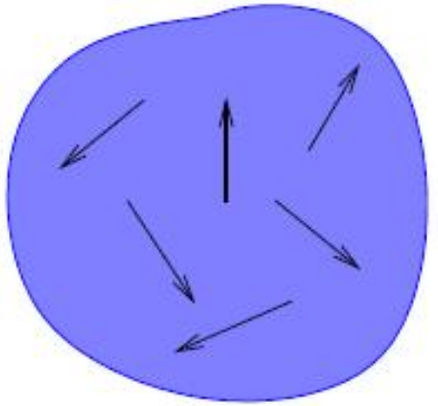

Lines are broadened because:

Energy levels themselves are not infinitely sharp

The atoms are moving relative to the observer

Three main mechanisms determine the profile of a spectral line:

1. Quantum mechanical uncertainty in the energy E of levels with finite lifetimes. This determines the ***natural*** width of a line, which is generally very small

2. Collisional broadening, most important in high-pressure environments (e.g. stars) where collisions are frequent. Collisions reduce the effective lifetime of a state, leading to broader lines

3. Doppler or thermal broadening, due to the motion of individual atoms in the gas relative to the observer. Larger scale turbulent motion can be treated in a similar way

Natural width

All energy levels except the ground state have a non-zero intrinsic width set by the uncertainty principle. For an energy level with energy E and lifetime Δt

$$\Delta E \; \Delta t \sim \hbar \tag{2}$$

short-lived states have large uncertainties in the energy. An atom makes a transition to the ground state. The emitted photon will then have a range of possible frequencies

$$\Delta \nu \sim \frac{\Delta E}{h} \sim \frac{1}{2\pi \; \Delta t} \tag{3}$$

Natural linewidth

If the spontaneous decay of an atomic state n proceeds at a rate

$$\gamma = \sum_{n'} A_{nn'} \tag{4}$$

where the sum is over all lower energy levels, then it can be shown that the line profile for transitions to the ground state is of the form

$$\phi(\nu) = \frac{\gamma/4\pi^2}{(\nu - \nu_0)^2 + (\gamma/4\pi)^2} \tag{5}$$

This is a Lorentzian or natural line profile.

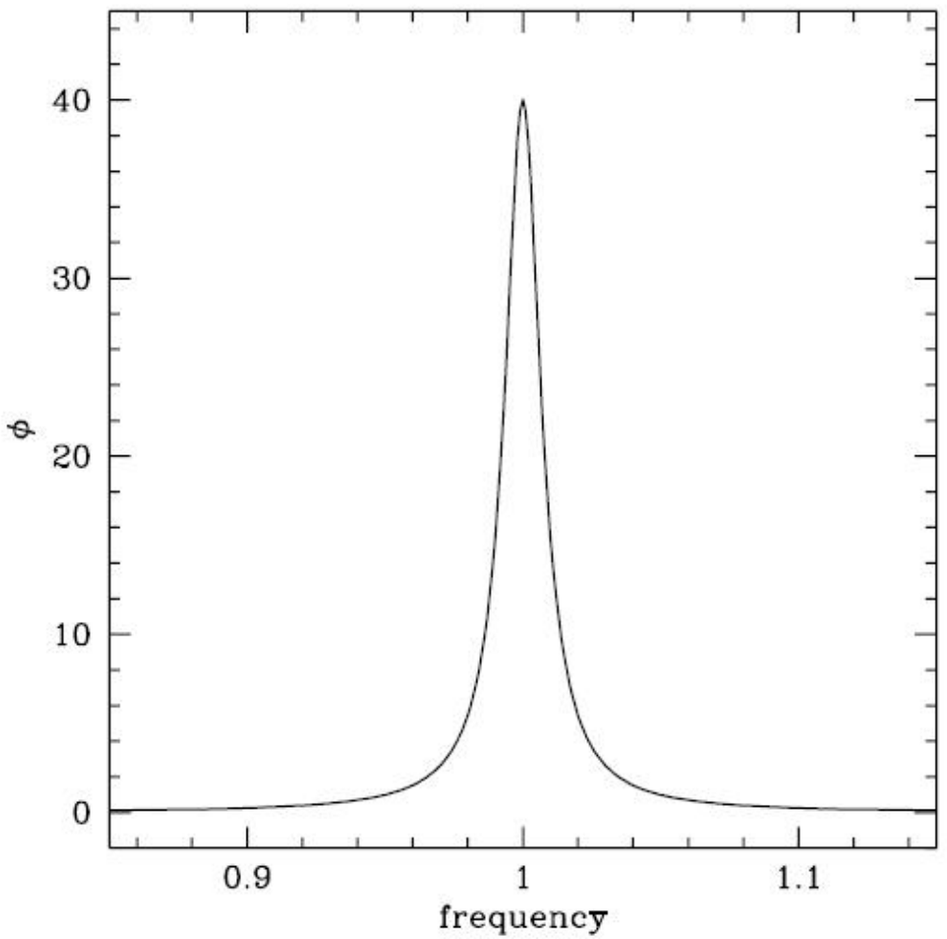

Figure 2: Well away from the line centre, the profile is proportional to ν^{-2}, a relatively *slow* decay - much slower than a Gaussian. Other effects normally broaden the centres of lines by more than the natural linewidth, not often directly observed, except in the line wings

Collisional broadening

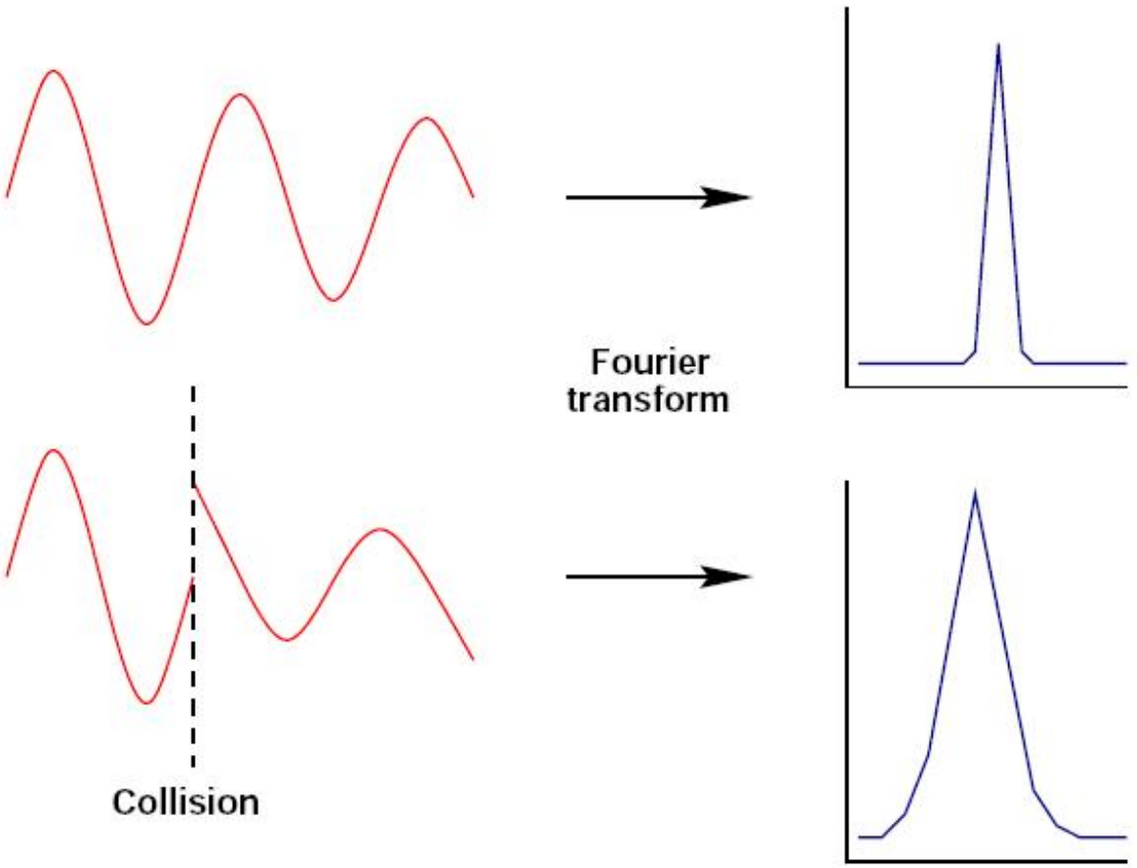

If collisions are frequent enough, they will randomize the phase of the emitted radiation and (effectively) shorten the natural lifetime further.

If the frequency of collision is ν_{col}, then the profile is

$$\phi(\nu) = \frac{\Gamma/4\pi^2}{(\nu - \nu_0)^2 + (\Gamma/4\pi)^2} \tag{6}$$

where

$$\Gamma = \gamma + 2\nu_{col} \tag{7}$$

Still a Lorentz profile. Collisions dominate in high density environments - hence get broader lines in dwarf stars than giants of the same spectral type.

Thermal broadening

Atoms in a gas have random motions that depend upon the temperature. The *most probable speed u* is

$$\frac{1}{2}mu^2 = kT \tag{8}$$

The number of atoms with a given velocity is given by Maxwell's Law of velocity distribution. Distinguish between forms for speed and for one component of v

one component, the distribution of velocities is described by a Gaussian

$$dN(v_x) \propto \exp\left(-\frac{mv_x^2}{2kT}\right)\, dv_x \tag{9}$$

The distribution law for speeds has an extra factor of v^2

$$dN(v) \propto v^2 \exp\left(-\frac{mv^2}{2kT}\right)\, dv \tag{10}$$

For thermal broadening the distribution for one component is relevant, since we only care about the motions along the line of sight

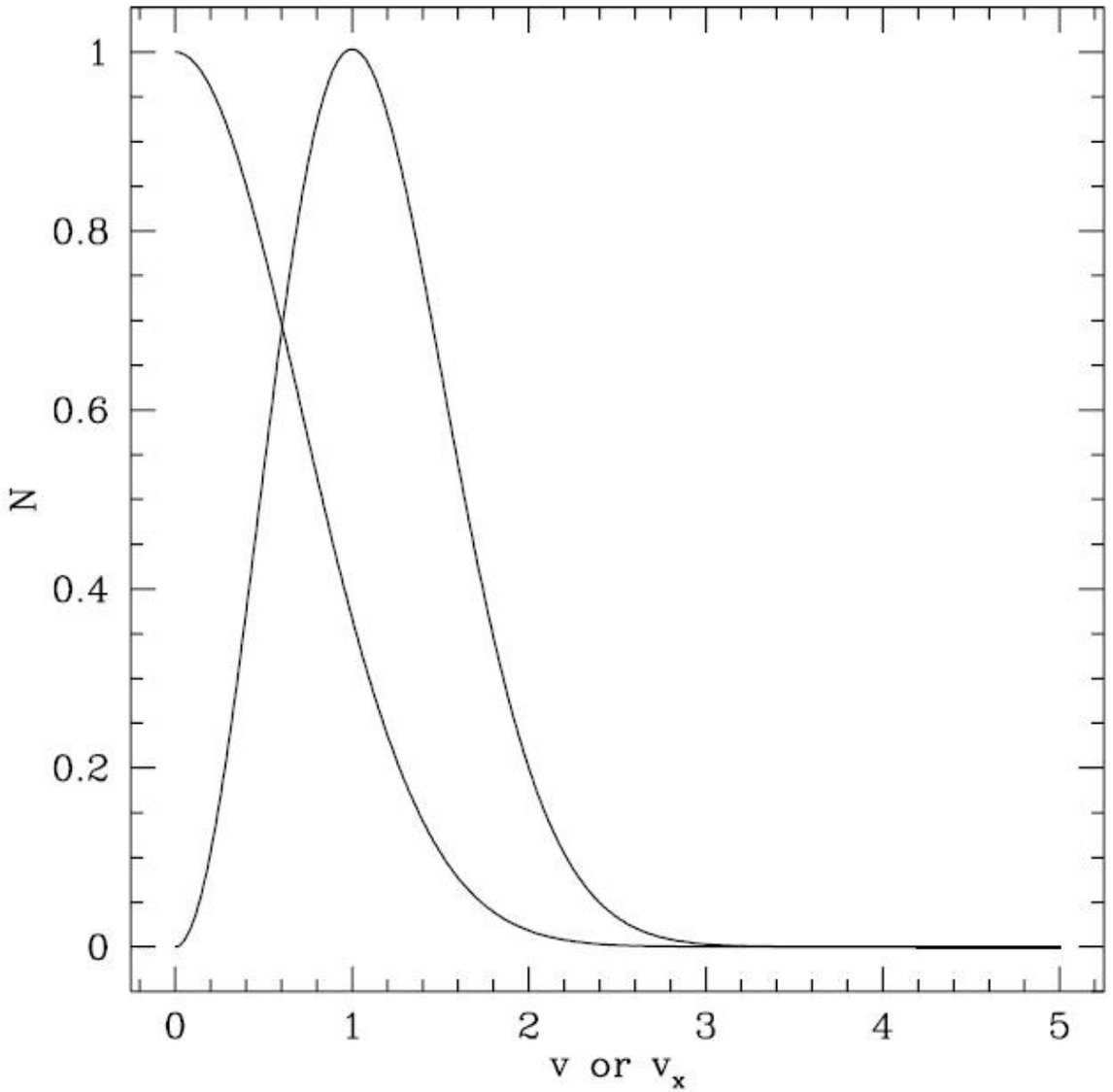

Figure 3: Maxwellian distributions of speed and velocity

Thermal broadening of spectral lines occurs because the frequency of emission or absorption for an atom in its own frame differs from that seen by an observer due to the Doppler effect. If ν_0 is the rest frame frequency, the observed frequency for an atom moving at velocity v_x along the line of sight is

$$\frac{\nu - \nu_0}{\nu_0} = \frac{v_x}{c} \tag{11}$$

Combining this Doppler shift with the one-dimensional distribution of velocities the profile function becomes

$$\phi(\nu) = \frac{1}{\Delta\nu_D \sqrt{\pi}} e^{-(\nu-\nu_0)^2/(\Delta\nu_D)^2} \tag{12}$$

where the ***Doppler width*** $\Delta\nu_D$ is defined as

$$\Delta\nu_D = \frac{\nu_0}{c} \sqrt{\frac{2kT}{m}} \tag{13}$$

If the gas has also turbulent motions that can be described by a similar velocity distribution, the effective Doppler width becomes

$$\Delta\nu_D = \frac{\nu_0}{c}\sqrt{\frac{2kT}{m} + v_{turb}^2} \tag{14}$$

where v_{turb} is a RMS measure of the turbulent velocity (star forming regions).

The thermal line profile is just a Gaussian, which falls off very rapidly away from the line centre. Numerically, for hydrogen the thermal broadening in velocity units is

$$\frac{\Delta\nu_D}{\nu_0}c = \sqrt{\frac{2kT}{m}} \simeq 13\ (\frac{T}{10^4 K})\ km\ s^{-1} \tag{15}$$

For the transitions of interest, the typical width of the Lorenzian is tiny, $\Delta\lambda \sim 10^{-4}$ Å full-width-half-maximum (FWHM) at ν_0=10^{14} Hz, or 0.006 km sec^{-1} at 5000 Å. Thus the natural line width is much smaller than the thermal width of the absorbing Maxwellian velocity distribution of the atoms in the absorbing cloud, the instrumental line width, or the turbulent cloud velocity dispersion.

Voigt profiles

The combination of the thermal broadening with the natural or collisionally broadened line profile is called the Voigt profile. This is the convolution of the Lorentz profile with a Doppler profile, which results in a cross-section for absorption described by the Voigt integral

$$\sigma_\nu = a_{\nu_o}\, H(a,x) \tag{16}$$

where $H(a,x)$ is the Hjerting function.

$$H(a,x) = \frac{a}{\pi} \int_{-\infty}^{\infty} \frac{exp(-y^2)}{(x-y)^2 + a^2} dy \tag{17}$$

and

$$a_{\nu_o} = \frac{\sqrt{\pi} e^2}{m_e c} \frac{f}{\Delta\nu_D} \tag{18}$$

where f is the oscillator strength. The dimensionless frequency x is

$$x = \frac{\nu - \nu_o}{\Delta\nu_D} = \frac{\lambda - \lambda_o}{\Delta\lambda_D} \tag{19}$$

the difference between the frequency or wavelength and the line center in units of the Doppler frequency or Doppler wavelength,

$$\Delta\lambda_D = \frac{\lambda_o^2}{c}\Delta\nu_D = \frac{\lambda_o}{c}\sqrt{\frac{2kT}{m_{atom}}} \tag{20}$$

The Voigt integral cannot be evaluated analytically and so is generated numerically. Humlicek (1979) gives a fortran subroutine for $H(a,x)$, and numerical tables are given by Finn & Mugglestone (1965). In the quasar absorption line literature, the programs *VPFIT* and *FITLYMAN* are in widespread use for fitting Voigt profiles. *VPFIT* was developed by Bob Carswell and several generations of students, who have generously made it available to the community (Carswell et al. 1995). *FITLYMAN* is described by Fontana and Ballester (1995).

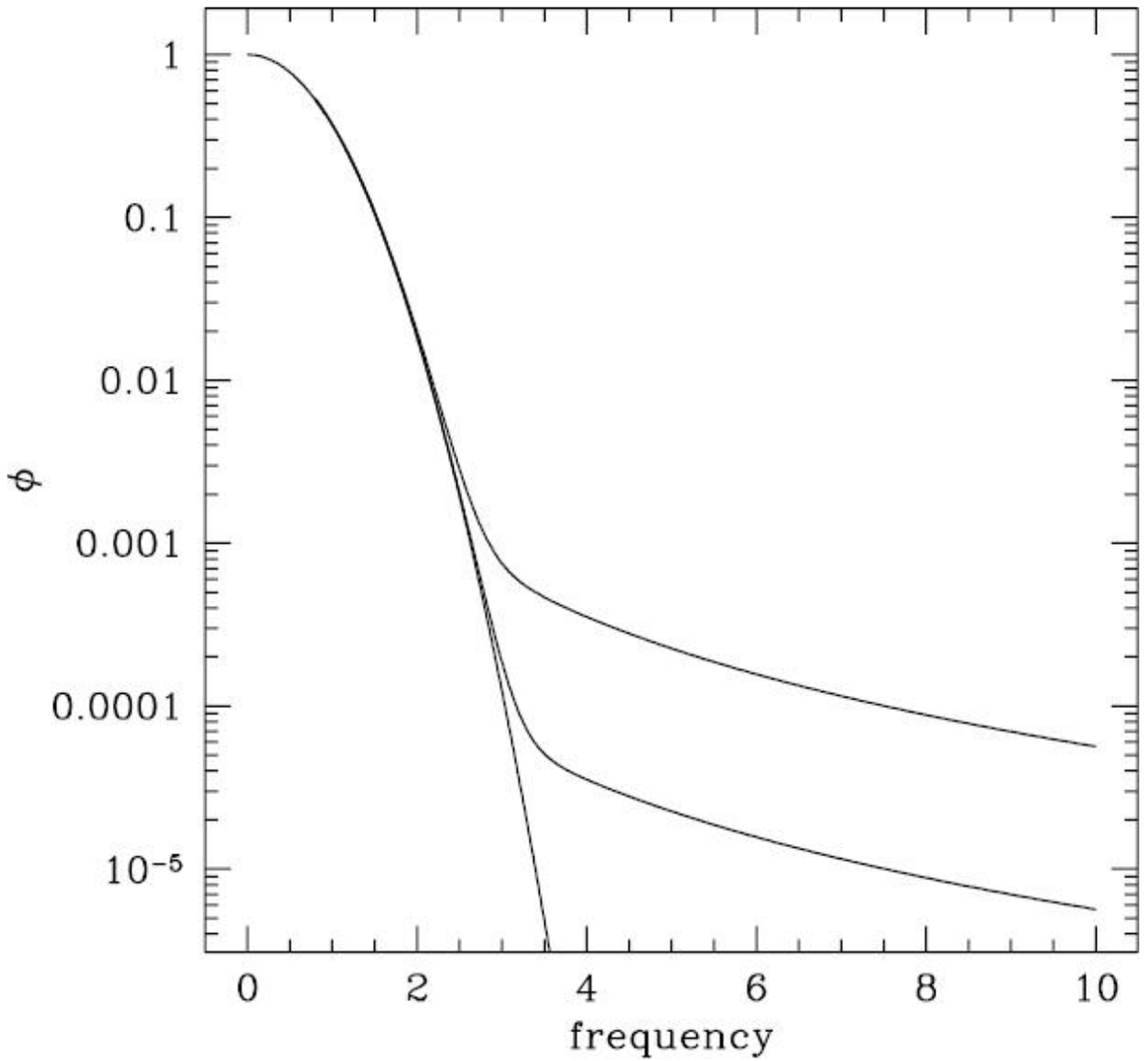

Figure 4: Theoretical Voigt profiles. The curves show the profile as the natural (or collisional) linewidth is increased. The Lorentz profile falls off slower than a Doppler profile, so typically the core is approximately Gaussian, while the wings look like a Lorentz profile.

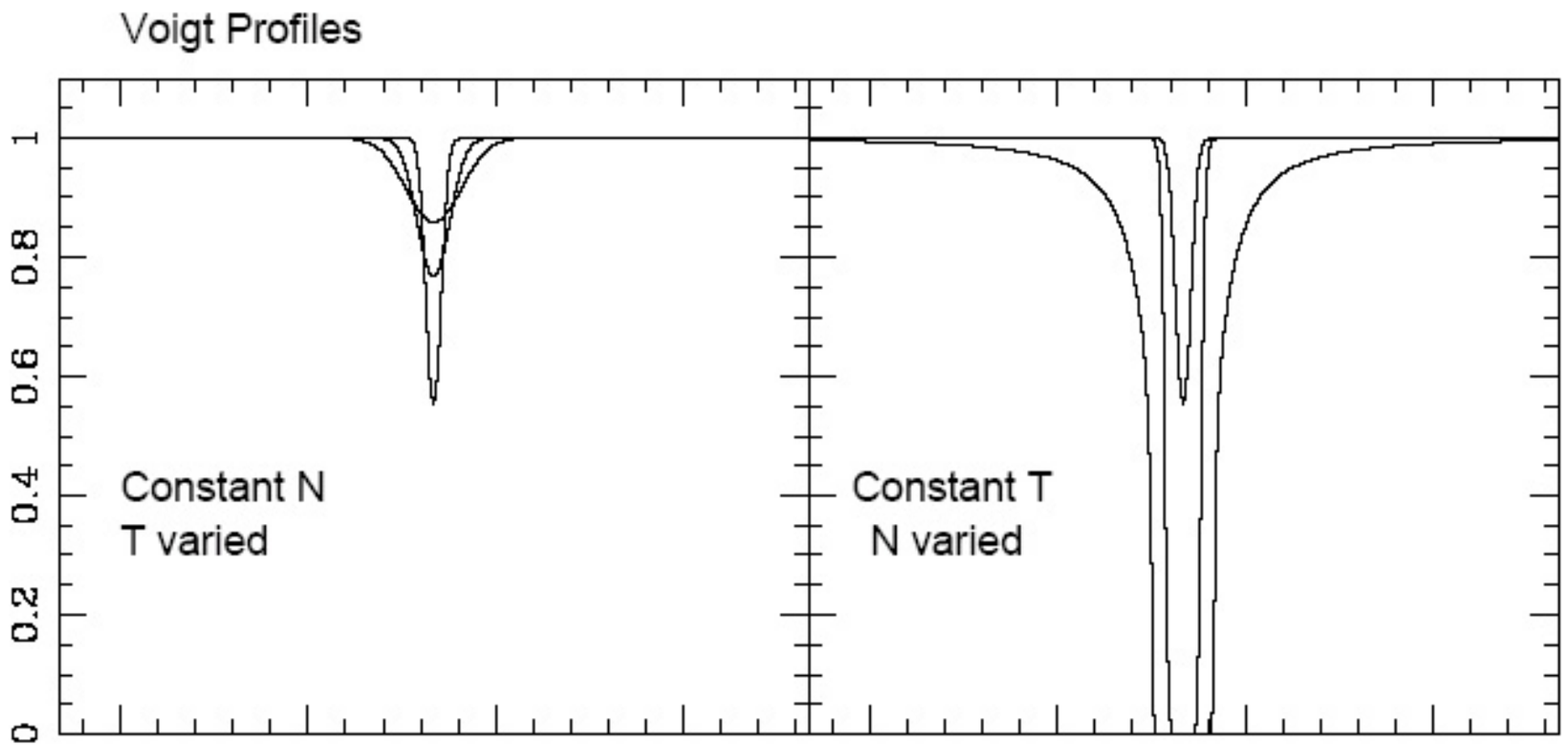

Figure 5: Theoretical Voigt profiles. Left side shows lines on the linear part of the curve of growth, $\tau_{\nu_o} < 1$, for constant column density N and $T = 10,000$; 50000 and 150000 K. Right hand side shows profiles for constant T and increasing N: τ_{ν_o} =0.5, 23 (flat or saturated) and 23,000 (damped).

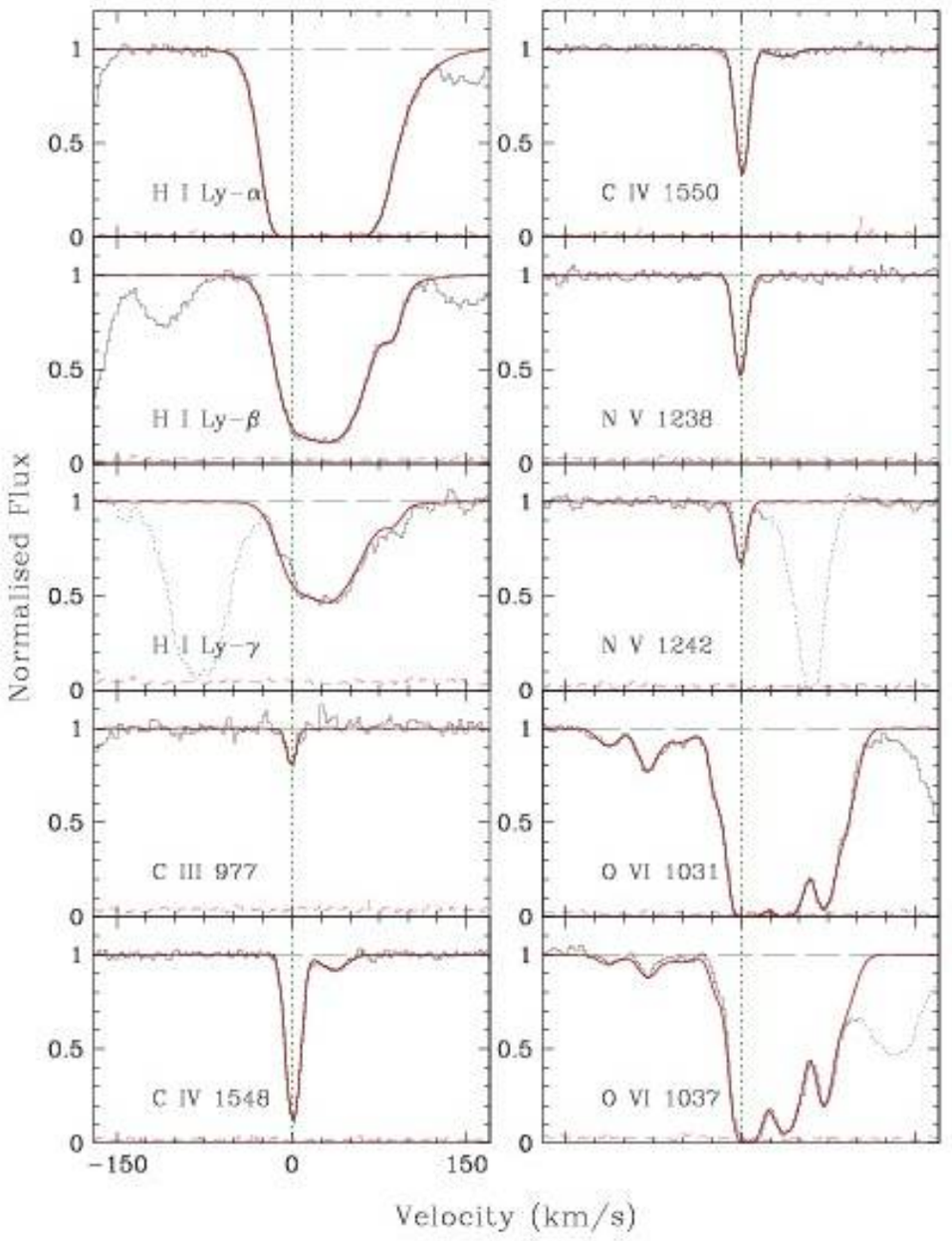

Figure 6: Example of a fit of a portion of a QSO spectrum. Data from D'Odorico, Cristiani, et al. 2004.

The observed line profile depends on the dimensionless optical depth at line center, τ_{ν_0}, which is

$$\tau_{\nu_o} = \int n \, \sigma_{\nu_o} dl \tag{21}$$

where the right hand side is the integral through the absorbing cloud of the volume density n (units are cm^{-3}) times the cross-section σ_{ν_0} (units are cm^2) at line center for absorption. One can show that

$$\sigma_{\nu_0} = \frac{\sqrt{\pi} e^2}{m_e c} \frac{f}{\Delta \nu_D} \tag{22}$$

so if the volume density n is uniform, we can write

$$\tau_{\nu_o} = N \frac{\sqrt{\pi} e^2}{m_e c} \frac{f}{\Delta \nu_D} \tag{23}$$

where N is the ***column density*** with units cm^{-2}.

The column density N represents the number of atoms in a column of unit cross section in the direction of the target, and is related to the number density of atoms by

$$N = \int n \; dl \tag{24}$$

Note that the optical depth at line center, τ_{ν_o}, increases with increasing column density, and is higher for higher f-values. As the temperature of the atoms increases, τ_{ν_o} decreases. If $\tau > 1$ then the line is said to be saturated. Increasing the column density of a saturated line has little effect on the line except to make it slightly wider, so it is difficult to measure the column density when this is the case.

For most metal-line transitions, and typical interstellar conditions, $T \sim 10,000$ K, so that most metal lines have very narrow line widths. Because the line width is inversely proportional to the square root of the mass of the absorbing atom, hydrogen lines are much wider for the same temperature.

Equivalent Width

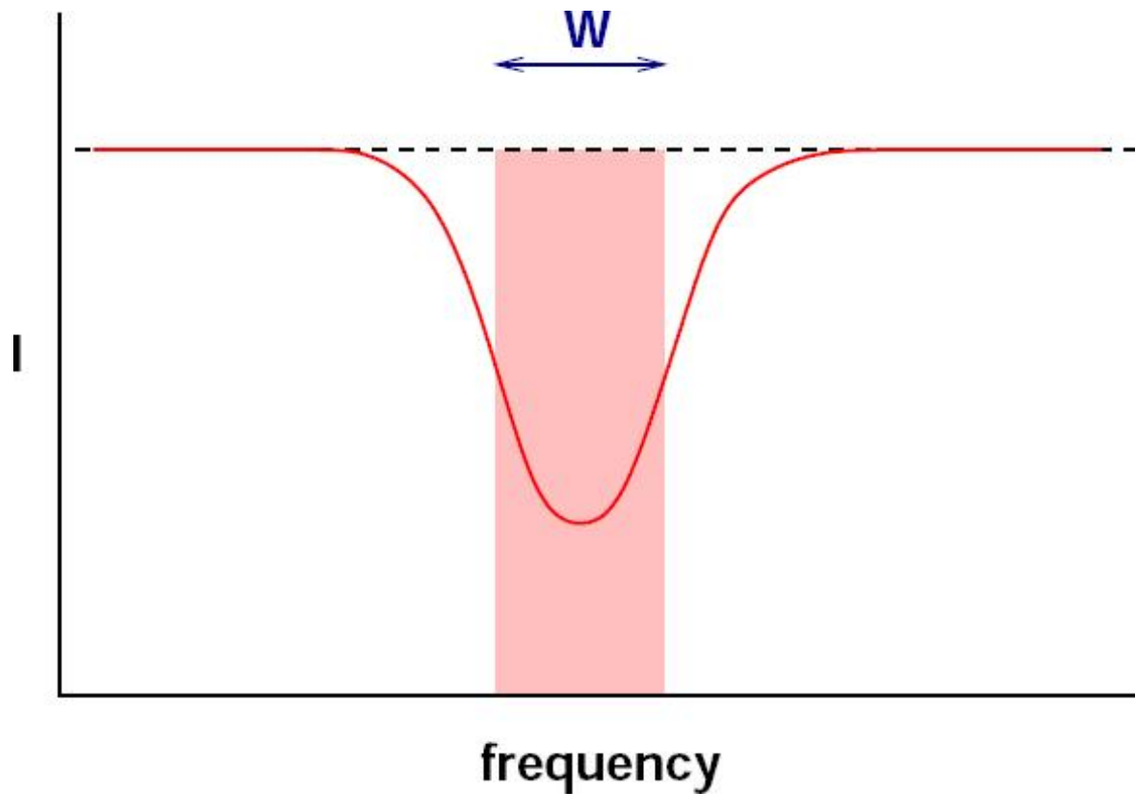

If the spectral resolution of the data is not good enough to resolve the line profiles, we can still learn a lot by measuring the “equivalent width" of the absorption line, which is defined as the width of a rectangular line with area equal to the absorbed area of the actual line (and typically is expressed with units of wavelength).

Equivalent Width

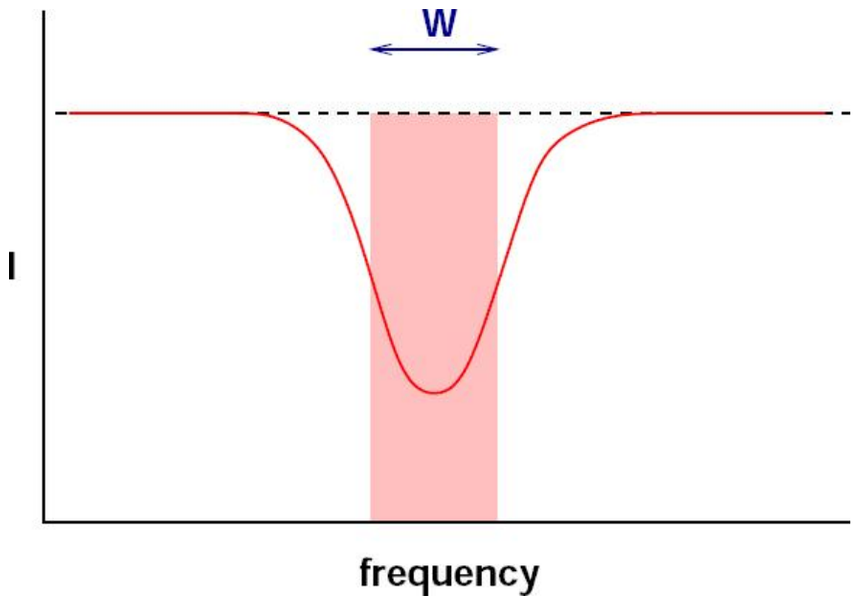

$$W(N) = \int (1 - \frac{I(\lambda)}{I_0})\, d\lambda \tag{25}$$

The EW reduces the information to one number, proportional to the area of the line, or its strength; the line profile information is lost. However, if you measure lines from the same ion with different f-values, then you can construct a “curve-of-growth" and deduce the column density, N, and temperature, T, of the ions.

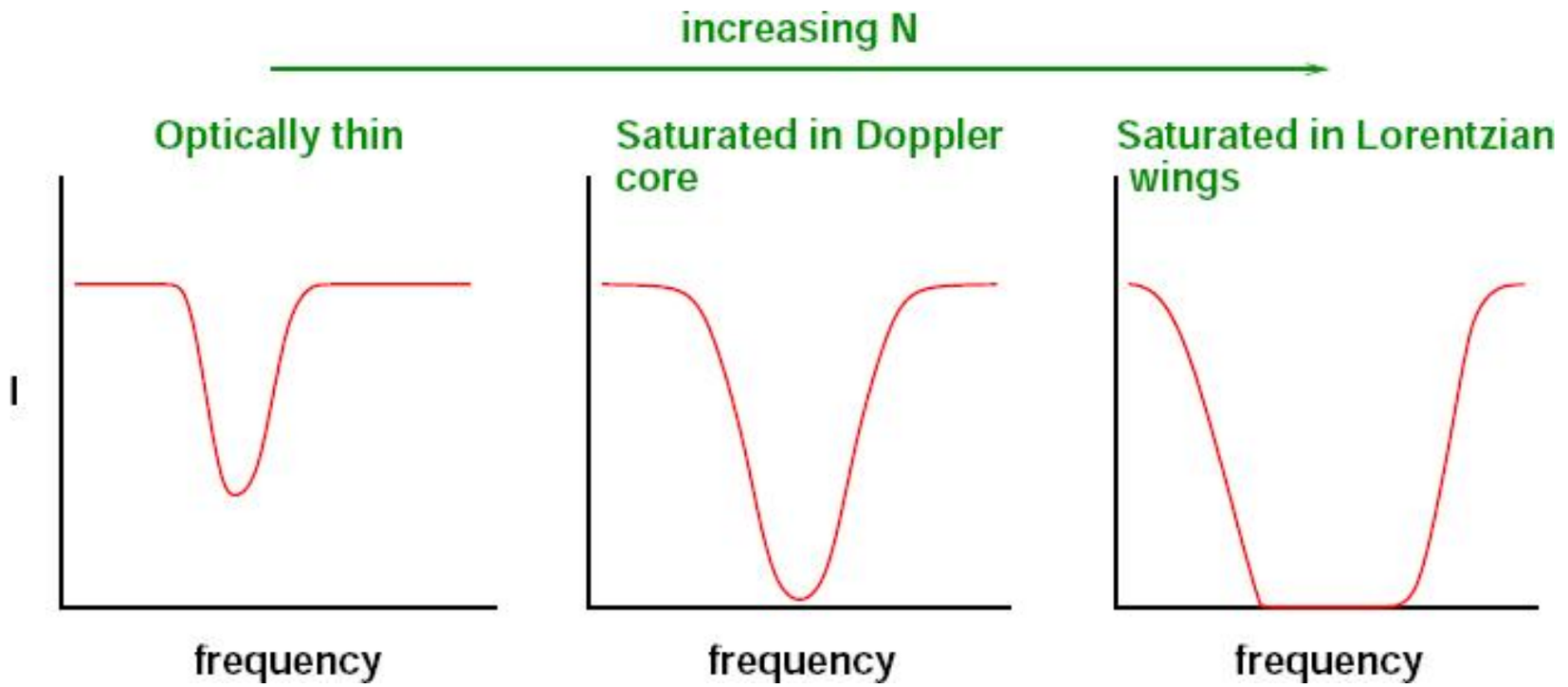

As N increases, the EW of the line also increases. The dependence of W upon N is non-trivial, because the flux in the line core cannot be less than zero the line becomes *saturated*.

EW three regimes.

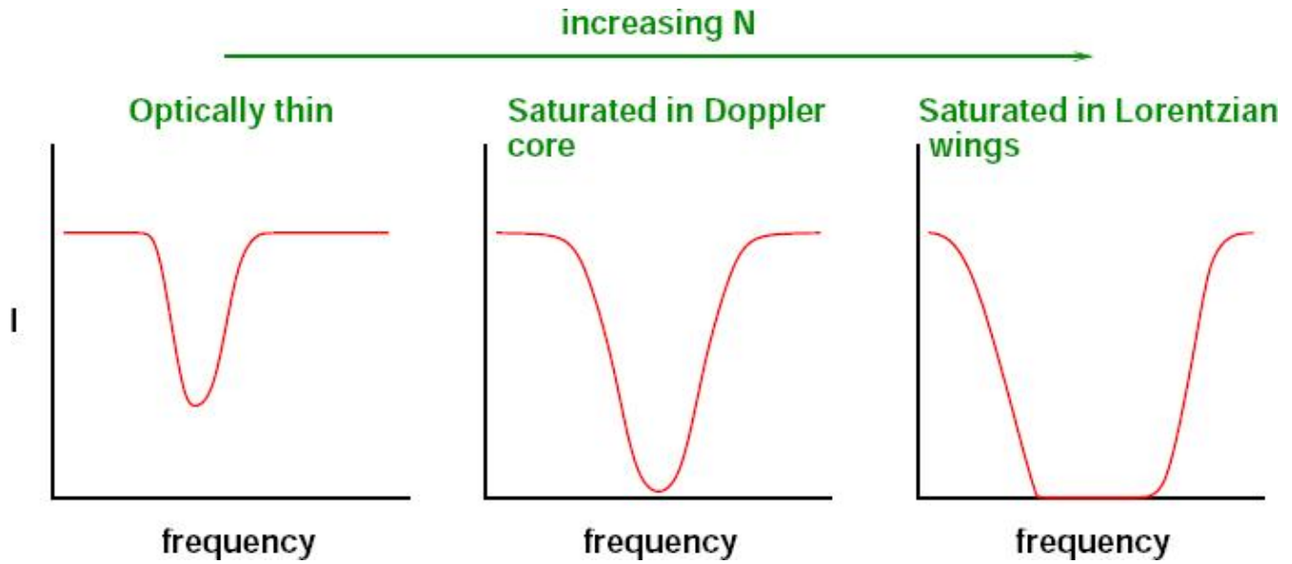

As column density increases, the line is:

1. Initially optically thin everywhere

2. Saturated in the core of the line. For a Voigt profile this part of the profile is determined by the Doppler broadening

3. Saturated out to frequencies/wavelengths where the line profile is determined by the Lorentzian wings

Different lines of a single species may fall in different regimes because their oscillator strength is different. The intensity after passing through the gas is

$$I(\nu) = I_0 \; e^{-\tau_\nu} = I_0 \; e^{-N \; \sigma_\nu} \tag{26}$$

where σ_ν is the absorption cross-section. If line optically thin at all frequencies, expand the exponential as a series $e^{-\tau} \simeq 1 - \tau$

$$W(N) = \int (1 - \frac{I(\nu)}{I_0}) \; d\nu \simeq \int N \; \sigma_\nu \; d\nu \propto N \; f \tag{27}$$

For very optically thick lines $\tau >> 1$ in the line centre, and τ changes rapidly with frequency once we get to $\tau \simeq 1$. Thus, the "edge" of the line is quite sharp and $W \sim 2 \; \Delta$, where Δ is the distance from the centre at which $\tau = 1$. Evaluating Δ gives:

$$W \propto \ln(N) \tag{28}$$

when the line saturates in the Doppler core (i.e. $\tau = 1$ is reached there), and

$$W \propto \sqrt{N} \tag{29}$$

when the line saturates in the Lorentzian wings.

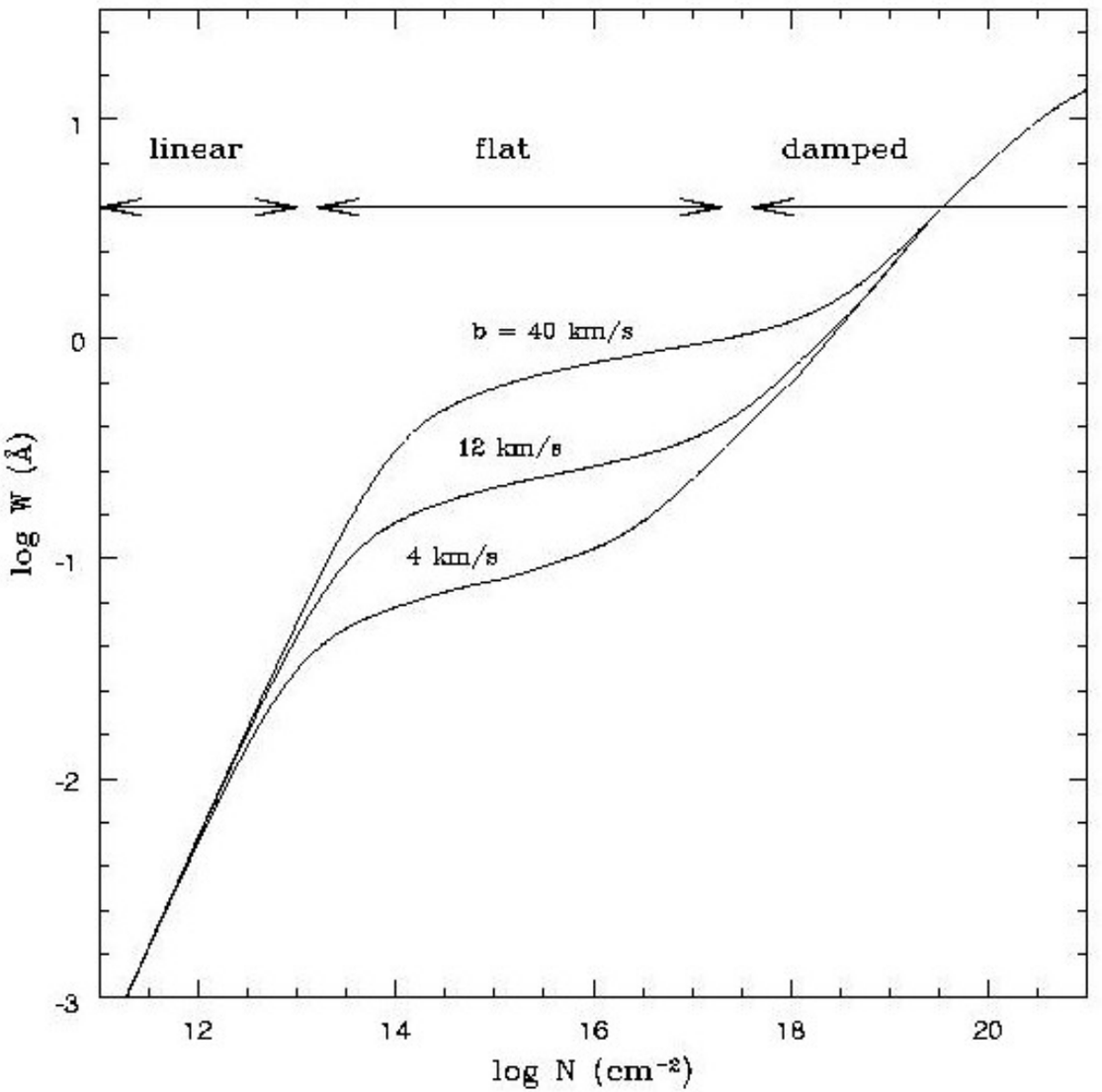

Figure 7: Theoretical curve of growth for Lyα. Equivalent width W in Å versus column density N. Linear, flat and damping parts of the curve of growth are indicated.

On the flat part of the curve of growth, the lines are saturated at center. EW is then insensitive to N but has some sensitivity to T, or equivalently, the b-value of the line, the so-called ***Doppler parameter***

$$b = \sqrt{\frac{2kT}{m}} \quad [km\ s^{-1}] \tag{30}$$

Rule of thumb: for a line on the linear part of the curve of growth

$$log(\frac{W_\lambda}{\lambda}) = log(\frac{N}{N_H}) + log\lambda f + logN_H - 20.053 \tag{31}$$

where W_λ is the EW, $\frac{N}{N_H}$ is the abundance of the atom relative to H, N_H is the total H column density and λ is the wavelength of the transition in Å.

UV absorption lines are very sensitive to small amounts of gas. Example: CIII (dominant ion for many interstellar clouds) has a strong line at λ=977 Å, with $f = 0.768$, so that log λ f = 2.876. The abundance, log C/H = -3.35 for solar abundance gas. One can easily detect a line with $W_\lambda = 0.1$, which corresponds to a log N_H = 16.5 cm^{-2}. This is a very small column compared to that easily probed by 21-cm or other emission line techniques. For Lyα, column densities of log N_H = 12.5 cm^{-2} are easily measured.

PROBABILITY TO GENERATE AN ABSORPTION

$$\frac{N_{obj}\ \sigma}{area} = \frac{N(V)\ V\ \sigma}{A} = N(V)\ \Delta l\ \sigma \quad \texttt{(all proper)}$$

$$P(l) \equiv N(V)\ \sigma \equiv \quad \texttt{prob. per unit length of the light path}$$

$$P(l)\ dl = P(z)\ dz$$

$$P(z) \equiv N(z) = N(V)\ \sigma\ \frac{dl}{dz} \tag{32}$$

$$N(z) = N(V)\ \sigma\ \frac{c}{H_o\ (1+z)\ E(z)} = \frac{N_{co}(V)\ \sigma\ c\ (1+z)^2}{H_o\ E(z)} \tag{33}$$

$$\Omega_\Lambda = 0,\ \Omega_R = 0 \Rightarrow \frac{dl}{dz} = \frac{c}{H_o}(1+z)^{-5/2} \Rightarrow \propto (1+z)^{1/2}$$

$$\Omega = 0,\ \Omega_R = 1 \Rightarrow \frac{dl}{dz} = \frac{c}{H_o}(1+z)^{-2} \Rightarrow \propto (1+z)$$

$$N_{co}(V)\ \sigma = N(z)\ \frac{H_o}{c}\ \frac{E(z)}{(1+z)^2} \tag{34}$$

OPTICAL DEPTH FOR GALAXY ABSORPTION

$$n_g \sim 0.02\ h^3\ Mpc^{-3}$$

$$r_g \simeq 10\ h^{-1}\ Mpc$$

$$\sigma = \pi r_g^2$$

$$\tau_i \simeq 0.01\ (1+z)^{3/2}\ \Omega^{-1/2} \quad \texttt{EdS} \tag{35}$$

$$\tau_i(z) = \int^z dP = \int dz\ \sigma\ n_o\ H_o^{-1}\ \frac{c\ (1+z)^2}{E(z)}$$

$$E(z) \propto \Omega^{1/2}\ (1+z)^{3/2} \qquad \texttt{EdS}$$

$$\tau_i(z) = \frac{\sigma\ n_o\ c}{H_o} \int \frac{(1+z)^2}{\Omega^{1/2}\ (1+z)^{3/2}}\ dz = \frac{2}{3}\ \frac{\sigma\ n_o\ c}{H_o\ \Omega^{1/2}}\ (1+z)^{3/2} \tag{36}$$

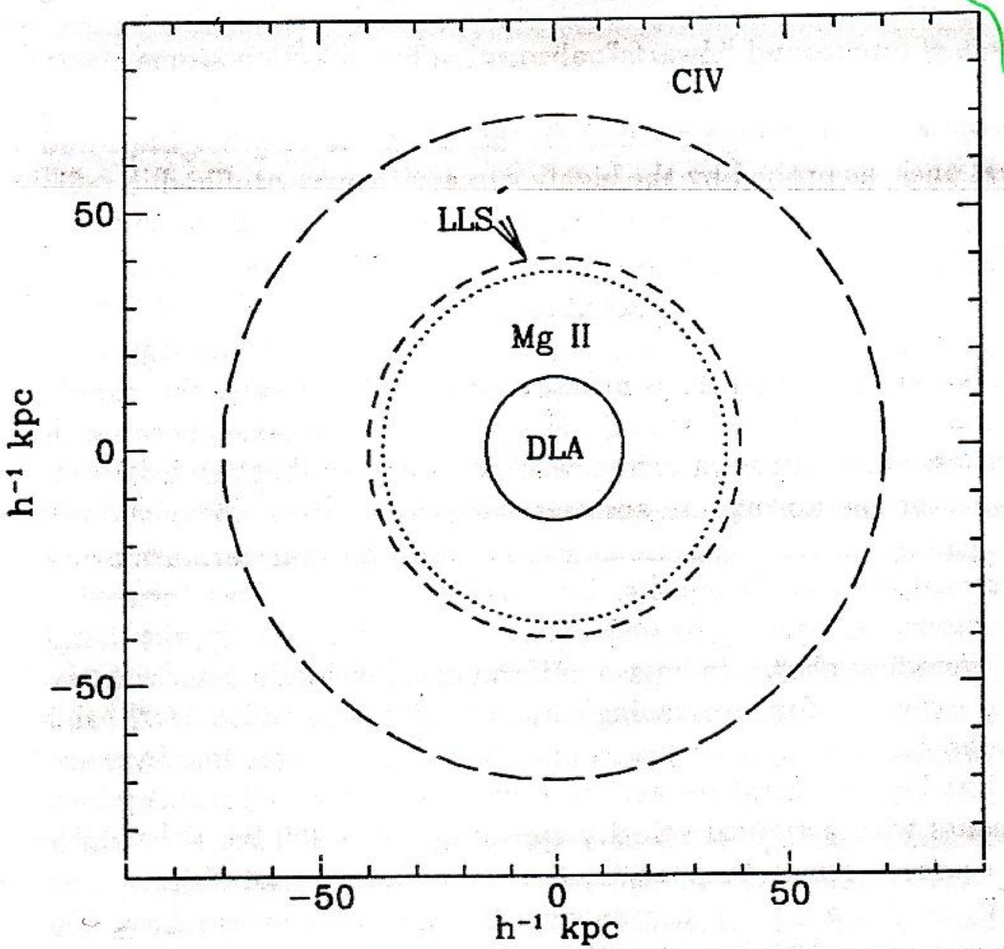

Fig. 1. Schematic diagram illustrating an over–simplified view of the structure of an "L^*" galaxy as deduced solely from the statistics of the various classes of metal line absorption systems. Note that the Mg II and Lyman limit selected systems have the same cross-section, and that the damped Lyman α systems have a cross–section which is only a few percent of the total.

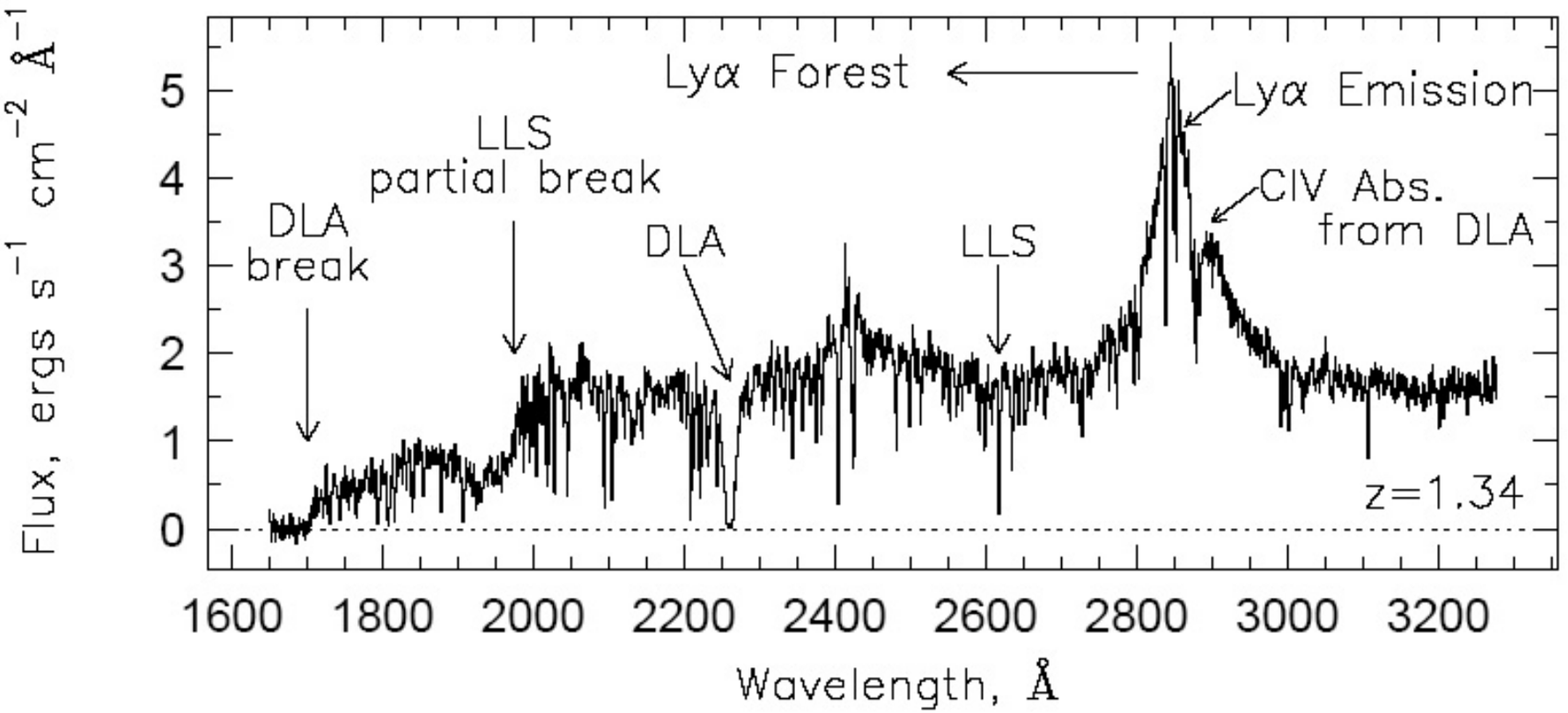
Flux, ergs s^{-1} cm^{-2} Å^{-1}
0
1
2
3
4
5
1600
1800
2000
2200
2400
2600
2800
3000
3200
Wavelength, Å
Lyα Forest
Lyα Emission
LLS
partial break
DLA
break
DLA
LLS
CIV Abs.
from DLA
z=1.34

Damped Lyman-α : examples

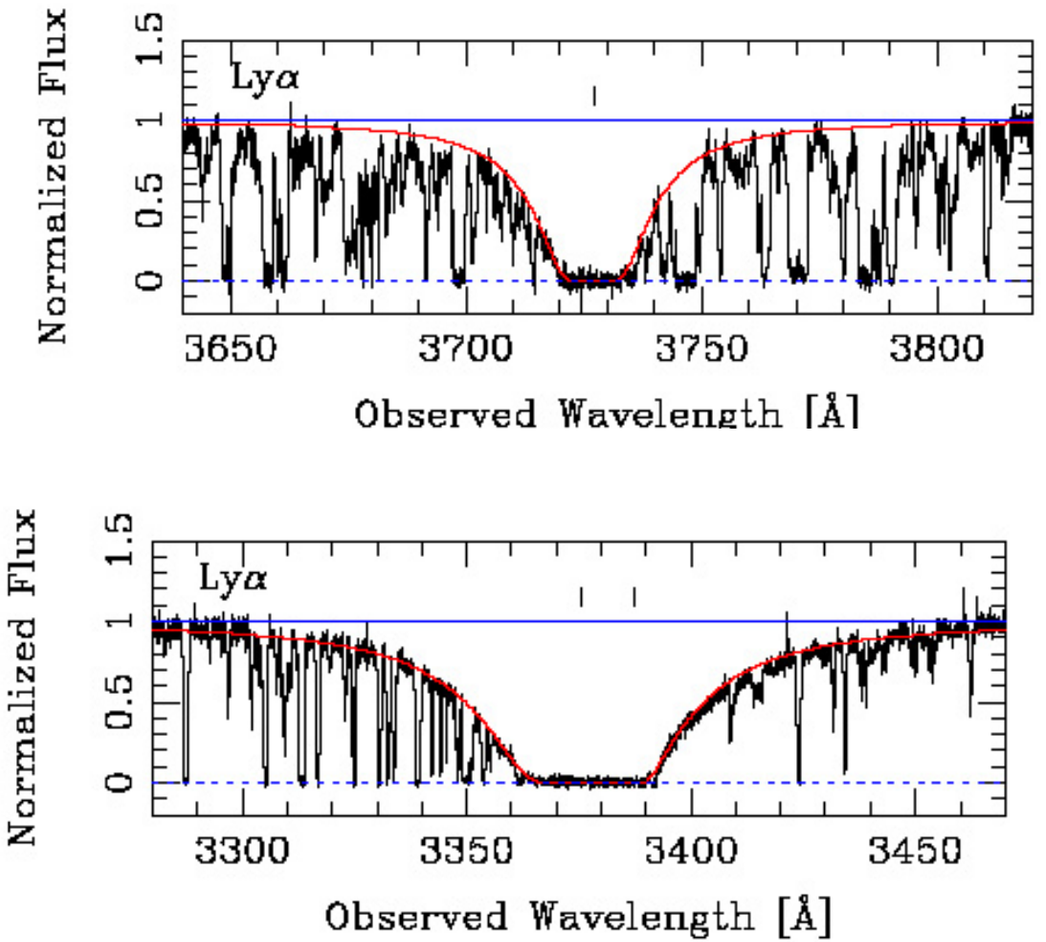

From Dessauges et al. 2004

Lyman Forest Early Models ('80)

Discrete Clouds

- Clouds ⇒Voigt Profiles ⇒Too Low Density & Too high ionization ⇒No star formation
- No metals & No clustering ⇒unrelated to galaxies

Pressure confined by a hotter and more tenuous ICM

PROBLEMS

- COBE limits on hot intra-cloud medium
- Range in N_{HI}- very large
- $N(z)$
- How did the clouds form??
- THE RISE OF DM MODELS
- High-res, high S/N spectra ⇒clustering, metallicity

- Cosmological hydro simulations

† R.I.P.

Dark Matter Models

large number of collapsed DMH too small to form stars and turn into galaxies

Warm photoionized IG gas sinks into mini-halos or accretes onto DM filaments and sheets

thermal gas pressure prevents further collapse

visible only in absorption

Dark Matter and Gas

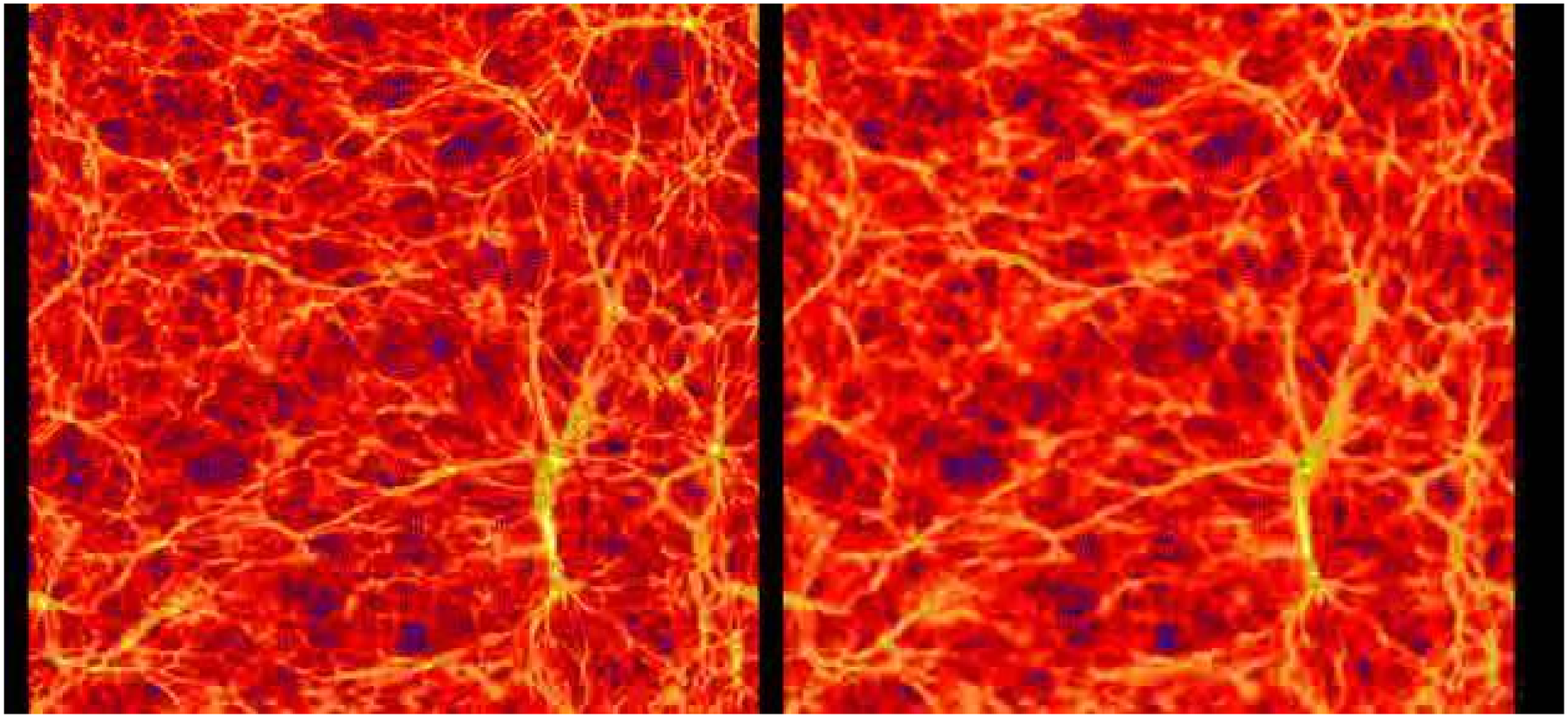

Figure 8: M.Viel et al. 2005

Stars and HI

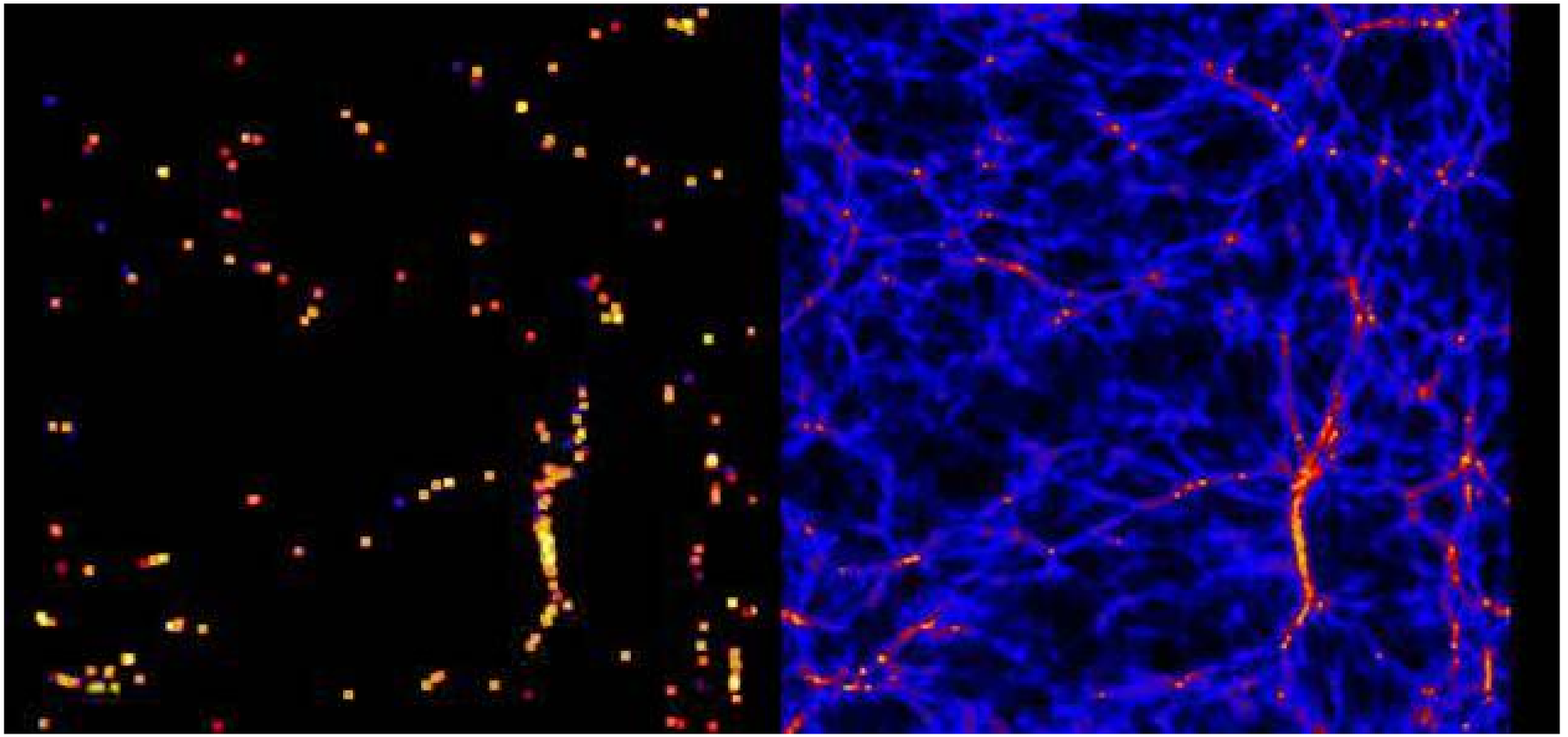

Cosmic Web

low-column density abs ($N_{HI} \leq 10^{14}$) associated with sheet-like structures or pancakes (length scale $\sim 0.1 - 1$ Mpc proper)

the gas accretes through weak shocks and settles in a dense, central cooling layer to form stars in some of the denser regions

at the lowest column densities gas remains unshocked, bounces back because of hydro pressure

higher and higher N_{HI} $\Rightarrow$ more and more spherical

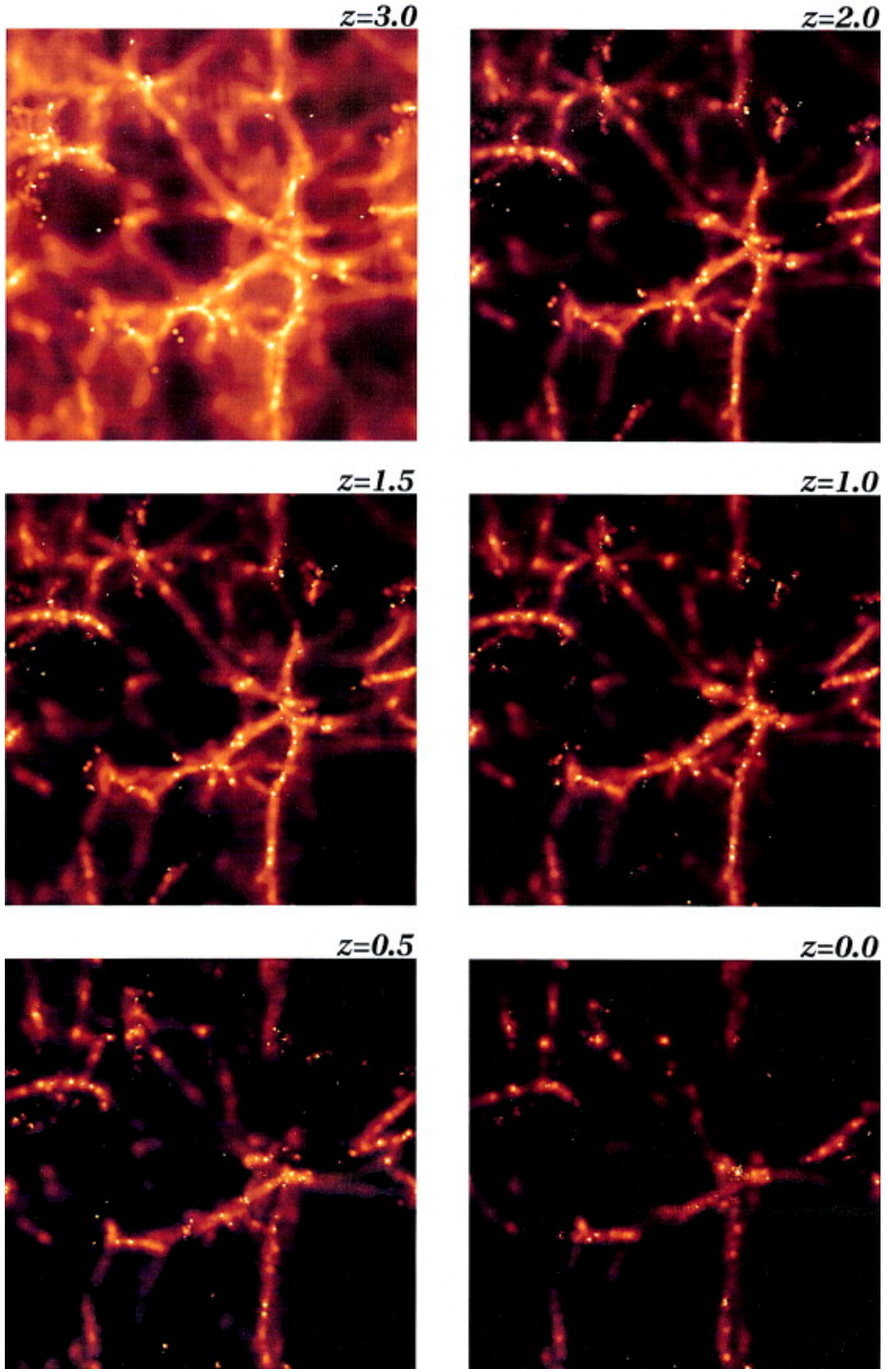

Figure 9: Davé et al. 1999 Red corresponds to $10^{13} < N_{HI} < 10^{14}$, orange $10^{14} < N_{HI} < 10^{15}$, yellow $10^{15} < N_{HI} < 10^{16}$, white $10^{16} < N_{HI}$

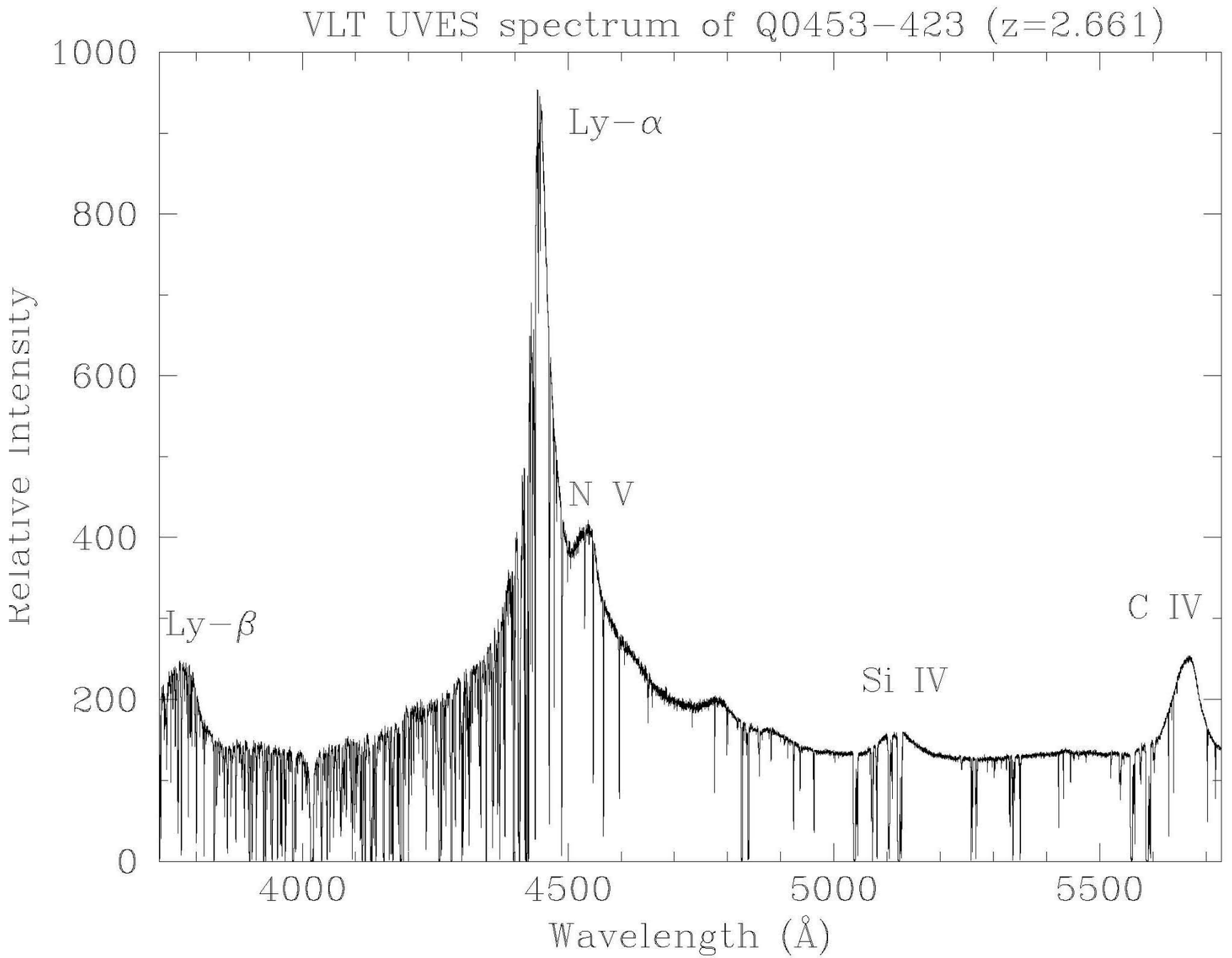
VLT UVES spectrum of Q0453−423 (z=2.661)
Relative Intensity
Wavelength (Å)
1000
800
600
400
200
0
4000
4500
5000
5500
Ly−α
N V
Ly−β
Si IV
C IV

INTERGALACTIC MEDIUM
Lecture 3
PROPERTIES OF THE LYMAN FOREST

Stefano Cristiani

cristiani@ts.astro.it

http://www.oat.ts.astro.it/~cristiani/

Lyman forest volution as a function of redshift

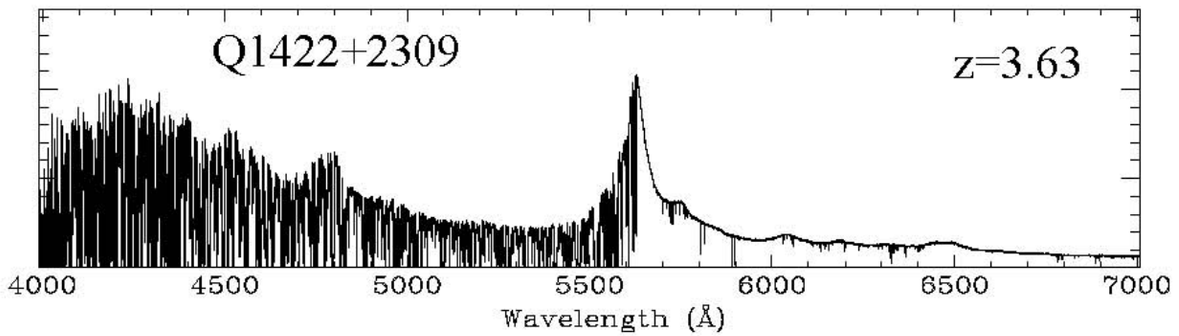

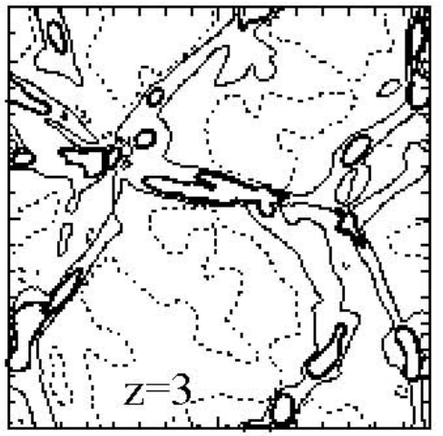

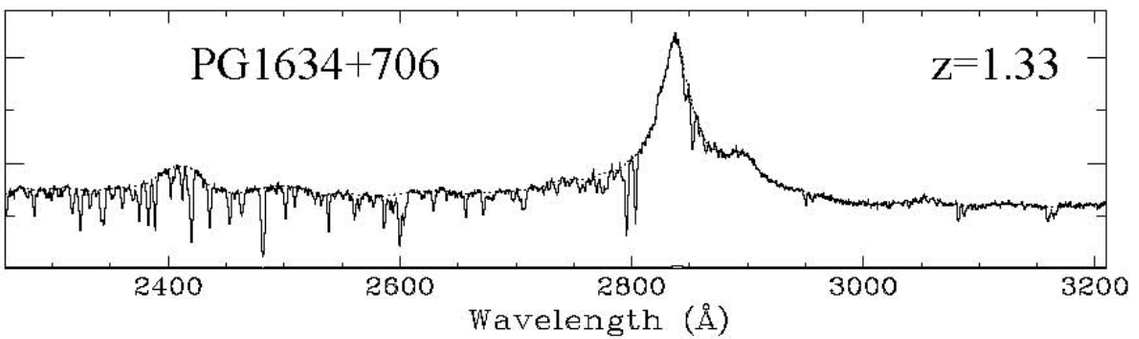

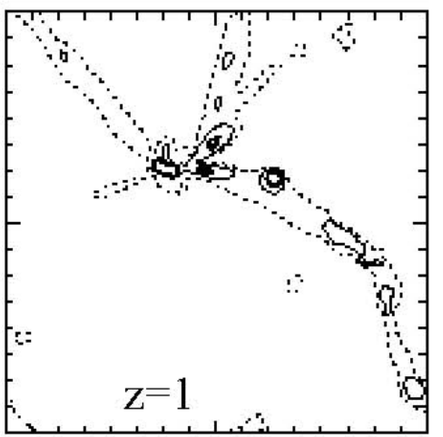

$$f_\lambda = f_c\, e^{-\tau_{HI}(\lambda)} \qquad e^{-\tau_{eff}} =< e^{-\tau} > \qquad \tau_{HI} \neq \tau_{eff} \qquad D_A =< 1 - \frac{f_\lambda}{f_c} > \quad (1)$$

Effective opacity as a function of redshift

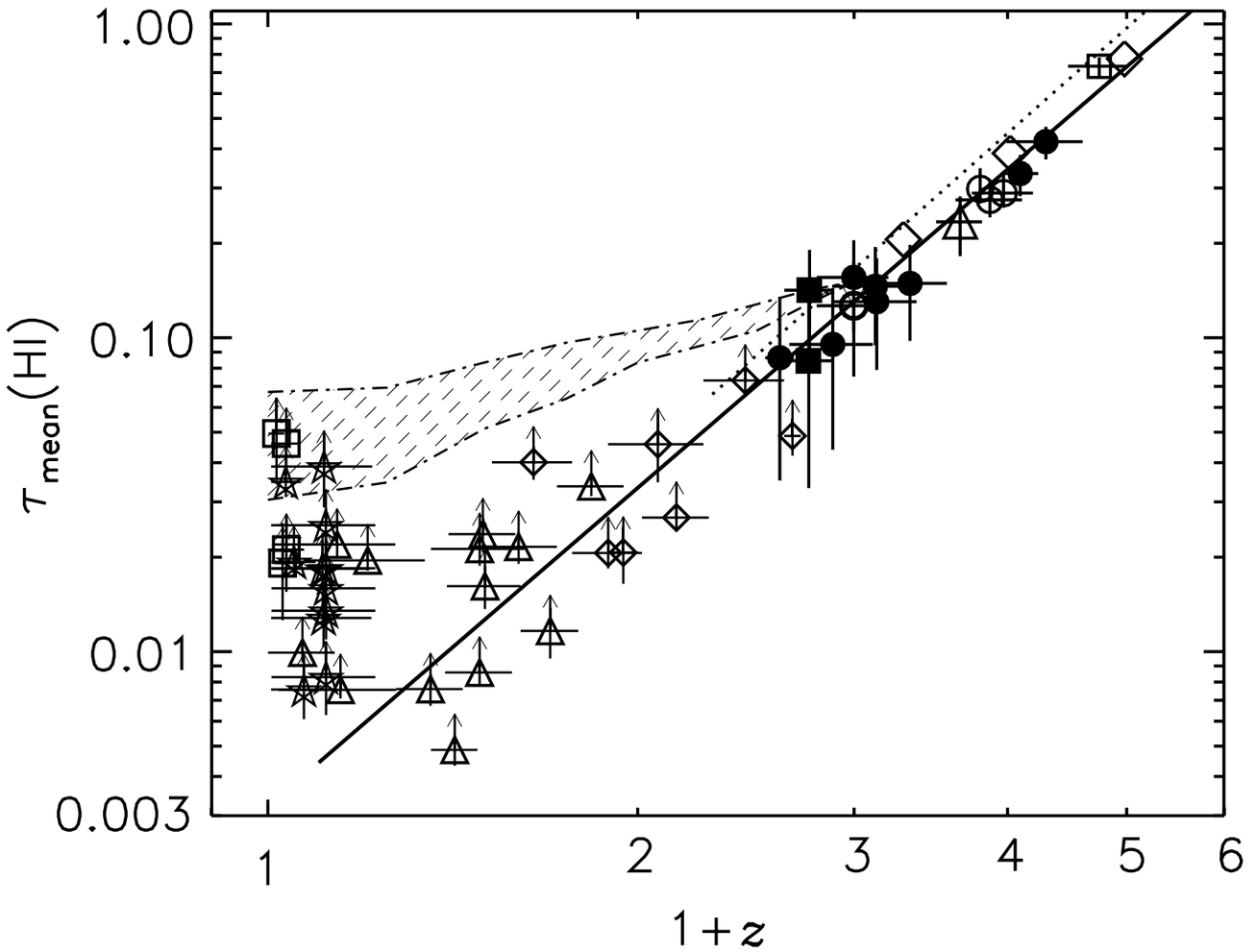

$$\overline{\tau}_{\rm HI}(z) = 0.0039 \pm 0.0009\,(1+z)^{3.4\pm0.2} \qquad (2)$$

The HI opacity as a function of z. Filled symbols represent the mean HI opacity from the UVES data. The open circle at $<z> = 2.0$ represents $\overline{\tau}_{HI}$ of J2233–606 when two high column density systems are excluded. Other symbols at $z > 1.5$ are from: open circles (Hu et al. 1995), large square (Lu et al. 1996), the open triangle (Kirkman & Tytler 1997), and diamonds (Rauch et al. 1997). Symbols at $z < 1.5$ with arrows are from: open diamonds (Impey et al. 1996), open triangles (Weymann et al. 1998), open stars (Impey et al. 1999) and open squares (Penton et al. 2000). Due to the low resolution and low S/N spectra of the ***HST*** observations, $\overline{\tau}$ could be highly underestimated if the Lyα forest at $N_{HI} \leq 10^{14}$ cm^{-2} contains the bulk of the neutral hydrogen. $\overline{\tau}_{HI}$ estimates, while the y-axis error bars were estimated from simply changing the adopted continuum by $\pm 5\%$. The dotted line represents the commonly used formula by Press et al. (1993), $\overline{\tau}_{\rm HI}(z) = 0.0037\,(1+z)^{3.46}$. The shaded area enclosed with dot-dashed lines indicates the ranges of $\overline{\tau}$ expected from different cosmological simulations by Davé et al. (1999).

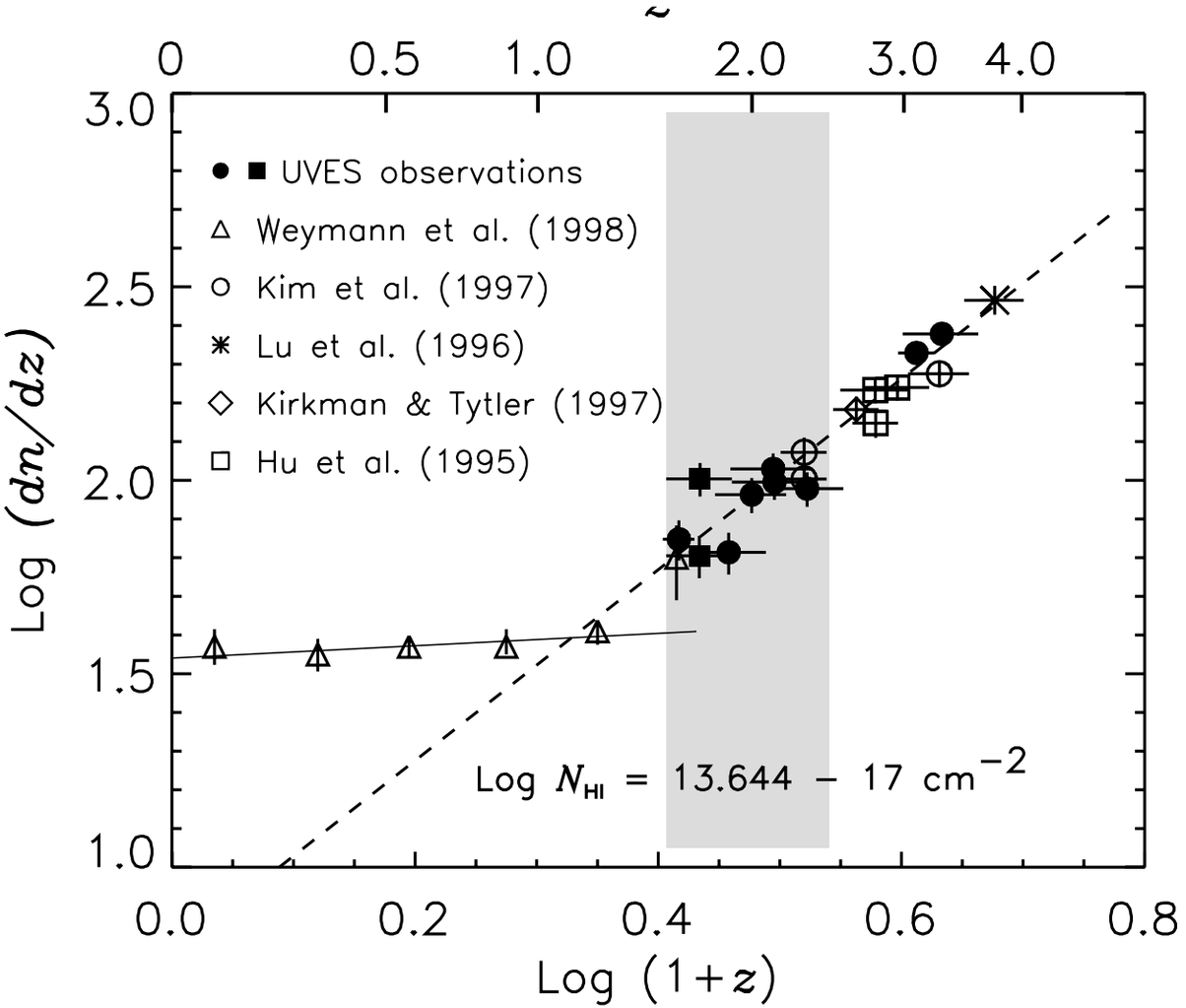

$$N(z) = N_o\,(1+z)^{\gamma} = 6.5\,(1+z)^{2.3\pm0.2} \qquad (3)$$

HST FOS KP EW> 0.24 expected $\gamma = 0.5 - 1 \Rightarrow$ EVOLUTION!!

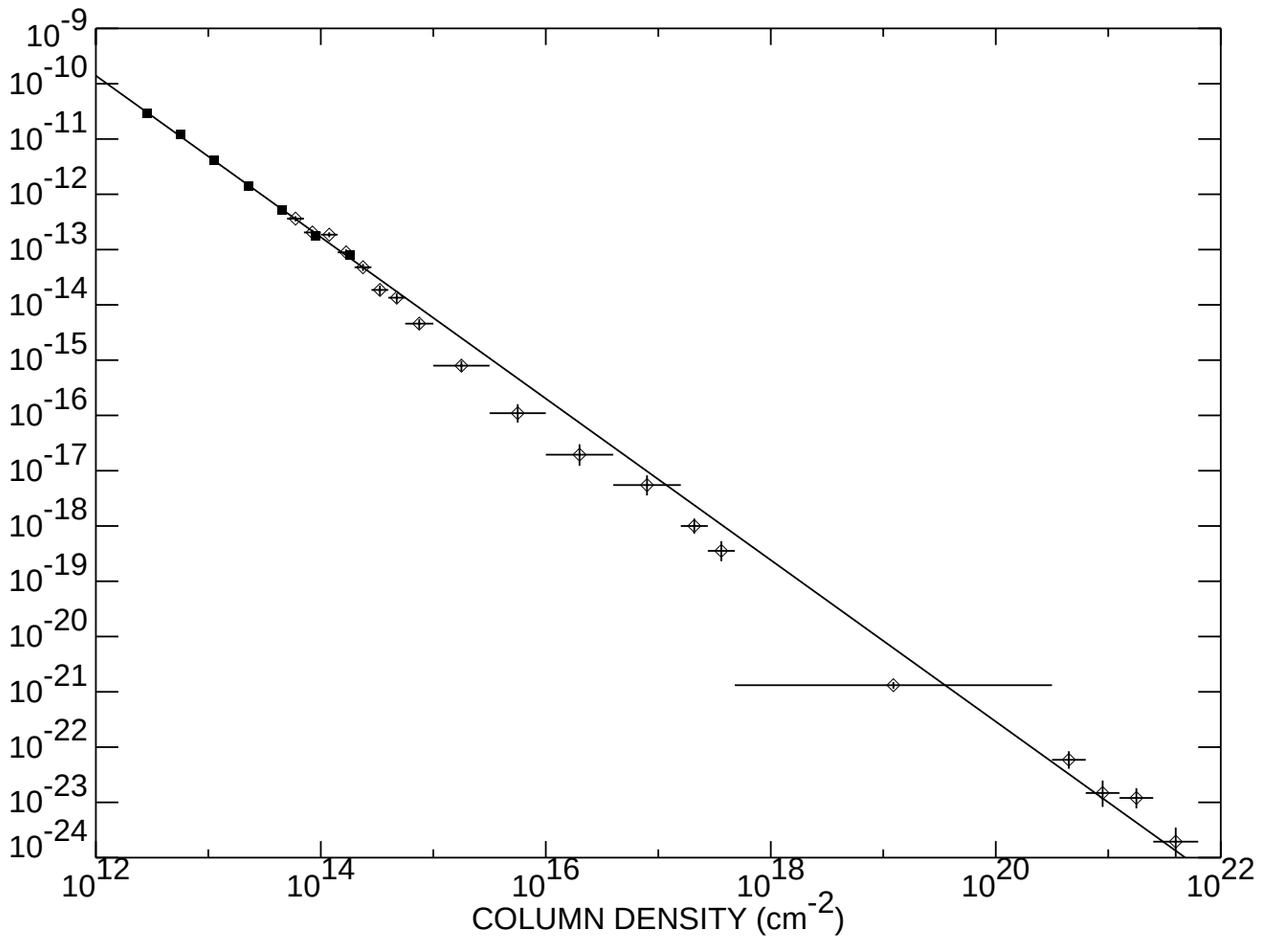

differential density distribution function ($\sharp$ of lines per unit redshift path and N_{HI})

$$f(N_{HI}) \propto N_{HI}^{-\gamma} \quad \gamma \simeq 1.5.$$

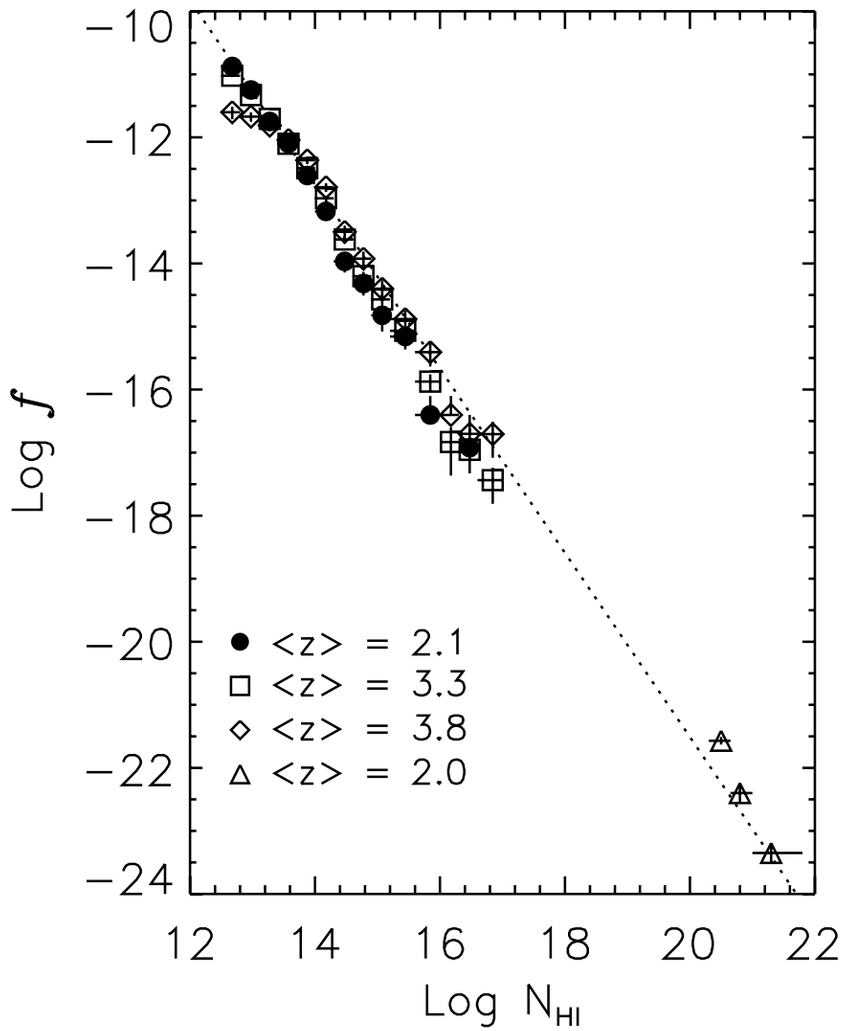

$f(N_{HI}) \propto N_{HI}^{-\gamma}$ $\gamma \simeq 1.5$ γ decreasing with z, $\gamma \simeq 2$ at $z \simeq 0.3$.

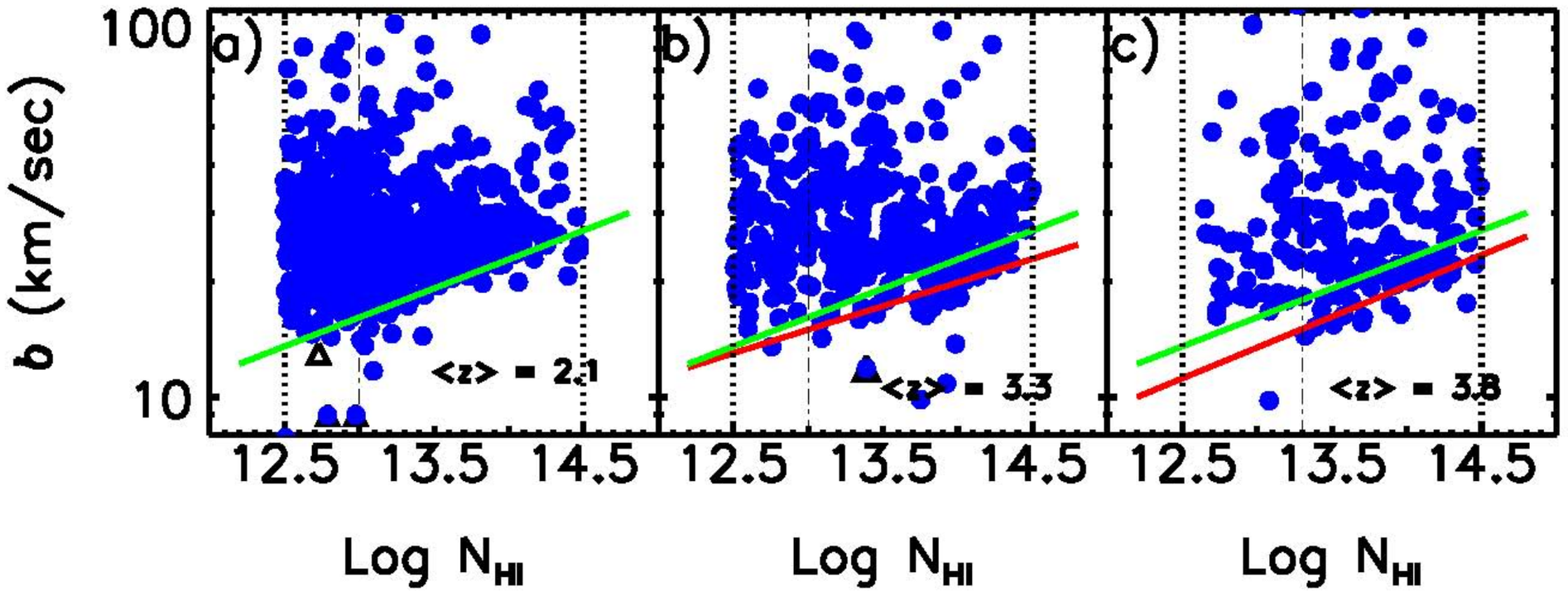

Doppler parameter vs. N_{HI} at various redshifts (Kim et al. 2001)

Analytical approximation of the $\aleph(z)$ evolution (Davé et al. 1999).

$$N(z) = N(V)\ \sigma\ \frac{c}{H_o\ (1+z)\ E(z)} = \frac{N_{co}(V)\ \sigma\ c\ (1+z)^2}{H_o\ E(z)}$$

$$\frac{dN}{dz} = \sigma_c \frac{dN}{dV_c}\ \frac{c}{H_o E(z)} \qquad E(z) = [\Omega_M(1+z)^3 + \Omega_R(1+z)^2 + \Omega_\Lambda]^{1/2}$$

gas distribution fixed in comoving coordinates

$$\rho(z) \propto (1+z)^3$$

$$HI\ fraction \equiv f \propto \frac{recombination\ rate}{photoionization\ rate} = \frac{n^2}{n\Gamma_{HI}(z)} = (1+z)^3\Gamma_{HI}^{-1}(z)$$

$$N_{HI} = N_H \cdot f \propto (1+z)^5\Gamma_{HI}^{-1}(z)$$

$$Distribution(N_{HI}) \equiv \frac{dN}{dN_{HI}} \propto N_{HI}^{-\beta}$$

$$\beta \approx 1.5 - 1.7 \text{ at } z \sim 1.5 - 4$$

The number of lines above a limiting column density is the integral of $f(N_{HI})$

$$\int_{N_{HI}}^{\infty} f(N_{HI}) = F(N_{HI,lim}) \propto N_{HI,lim}^{1-\beta}$$

With respect to a reference redshift z_r

$$N'_{HI,lim} = N_{HI,lim} \left(\frac{1+z_r}{1+z}\right)^5 \frac{\Gamma_{HI}(z)}{\Gamma_{HI}(z_r)}$$

$$\frac{N}{N_r} = \int_{N_{HI}(1+z)^{-5}\Gamma_{HI}(z)}^{\infty} N_{HI}^{-\beta} dN_{HI} / \int_{N_{HI}}^{\infty} N_{HI}^{-\beta} dN_{HI} = [(1+z)^5 \Gamma_{HI}^{-1}(z)]^{\beta-1}$$

$$\left(\frac{dN}{dz}\right)_{>W_{r,lim}} = C \left[(1+z)^5 \Gamma_{HI}^{-1}(z)\right]^{\beta-1} E^{-1}(z)$$

Who is producing the UV photons (Γ_{HI})?

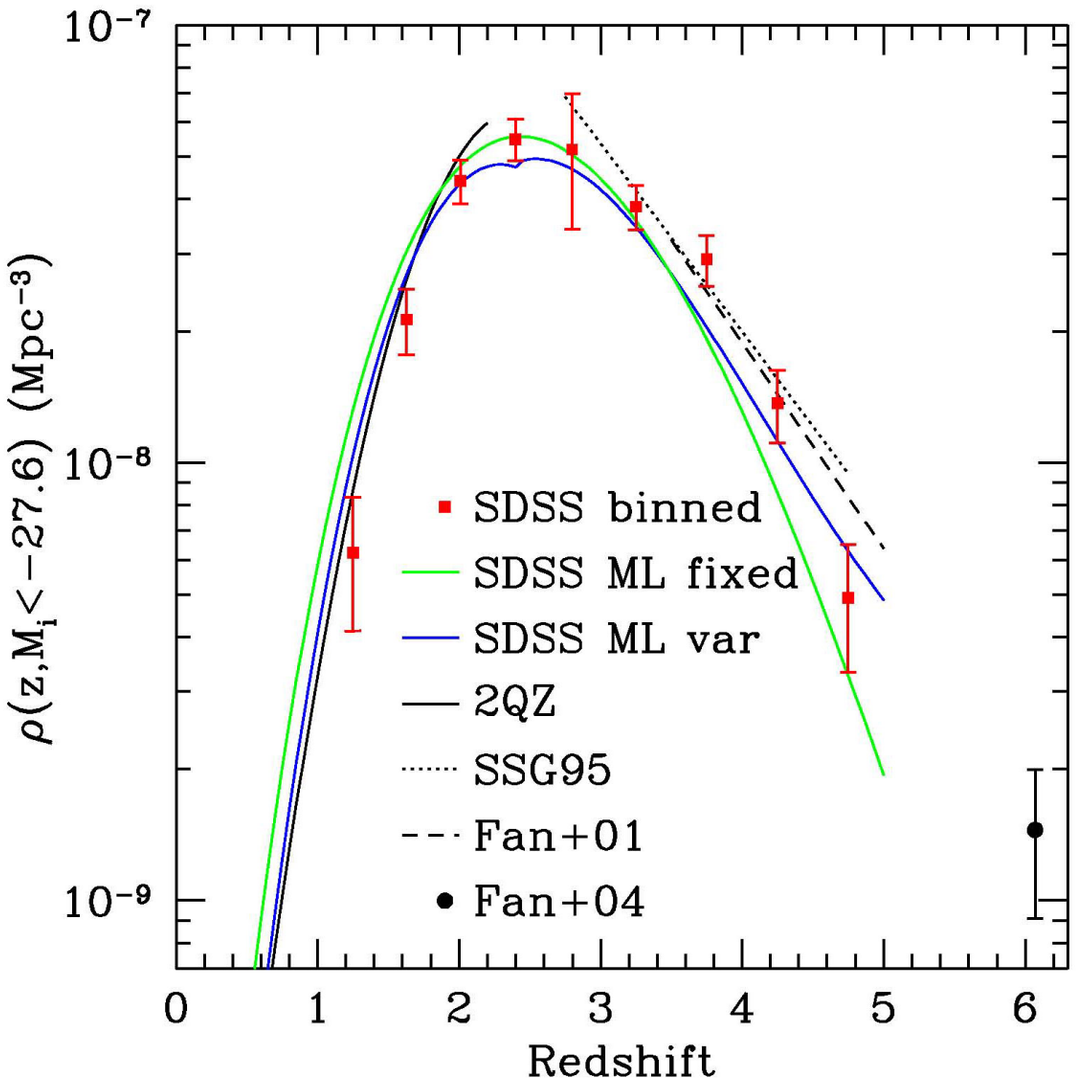

The space density of QSOs as a function of redshift (SDSS astro-ph/0601434)

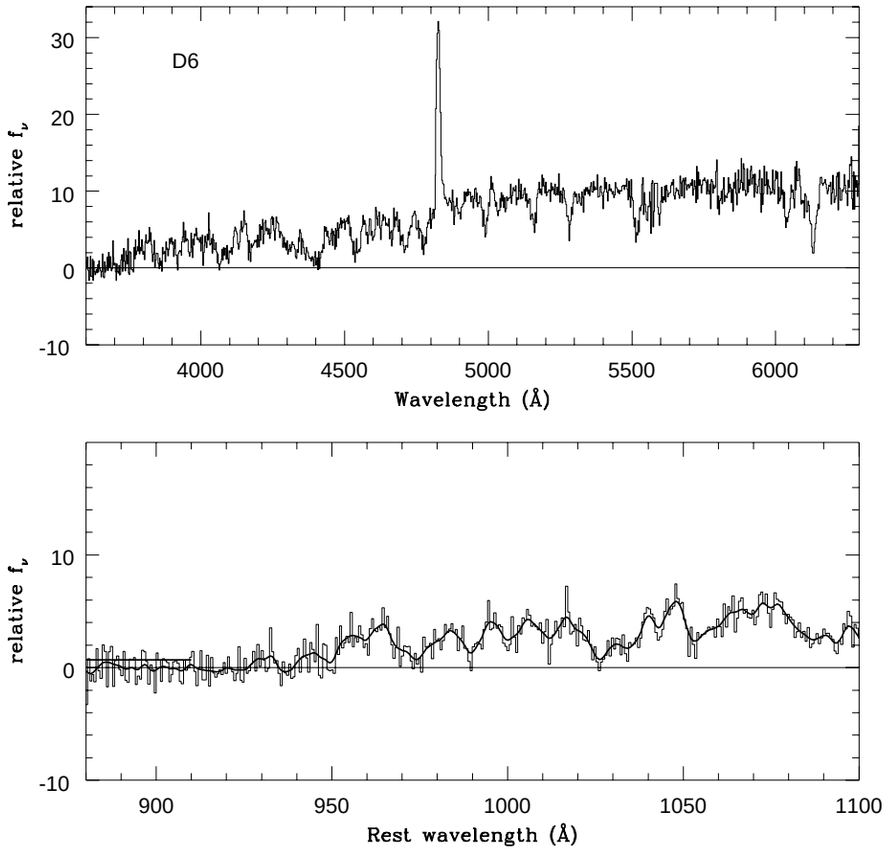

Giallongo, Cristiani, D'Odorico, Fontana 2002

1995MNRAS.273.1016C

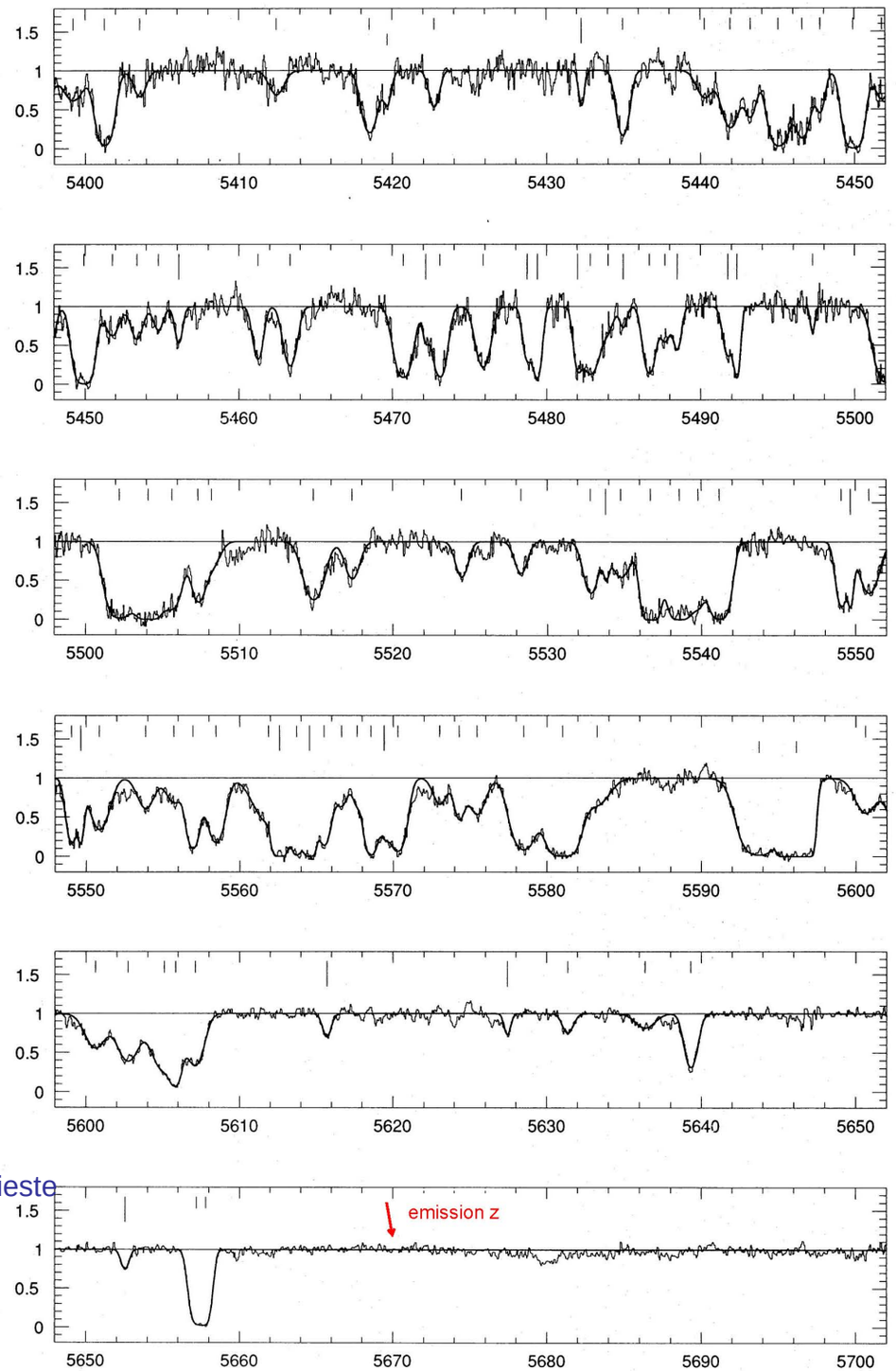

Figure 1 – *continued*

THE UV BACKGROUND FROM THE PROXIMITY EFFECT

Far away from the QSO

$$\frac{\partial^2 n}{\partial z \partial N_{HI}} = A_o (1+z)^{\gamma} \begin{cases} N_{HI}^{-\beta_f} & N_{HI} < N_{break} \\ N_{HI}^{-\beta_s} N_{break}^{\beta_s - \beta_f} & N_{HI} \geq N_{break} \end{cases} \quad (4)$$

Near the QSO

$$N_{HI} = \frac{N_\infty}{1+\omega} \qquad \omega(z) = \frac{F}{4\pi J}$$

(Bajtlik et al. 1988, Bechtold 1994)

Conservation Law

$$f(N) = g(N_\infty) dN_\infty / dN = g(N_\infty)(1+\omega)$$

$$\frac{\partial^2 n}{\partial z \partial N_{HI}} = A_o (1+z)^{\gamma} (1+\omega)^{1-\beta_f} \begin{cases} N_{HI}^{-\beta_f} & N_{HI} < N_{break} \\ N_{HI}^{-\beta_s} N_{break}^{\beta_s - \beta_f} & N_{HI} \geq N_{break} \end{cases}$$

where

$$N_{break}(z) = \frac{N_{\infty,b}}{1+\omega(z)}$$

Redshift Evolution

$$J = J_{(z=3)} \left(\frac{1+z}{4}\right)^{j}$$

Maximum likelihood analysis for lines with $\log N_{HI} \geq 13.3$ (ex. Giallongo et al. 1996)

N_l	γ	β_f	$\log N_{\infty,b}$	β_s	$\log J$	j
1128	2.49±0.21	1.10±0.07	14.00±0.02	1.80±0.03	-21.21±0.07	
	2.65±0.21	1.34±0.07	13.98±0.04	1.80±0.03	-21.32±0.08	–
	2.67±0.26	1.33±0.09	13.96±0.07	1.80±0.04	-21.32±0.10	-0.28±1.41

$J_{-22} = 5 \pm 1 \simeq$ the integrated contribution of QSOs

(Haardt& Madau 2001)

No evidence for redshift evolution

Possible sources of bias:

- same spectral shape for the UVB and the spectrum of individual QSOs
- QSO reside in overdensities
- magnification by gravitational lensing
- QSO variability
- The blanketing effects increases the rate of the redshift evolution: $\gamma = 2.65$

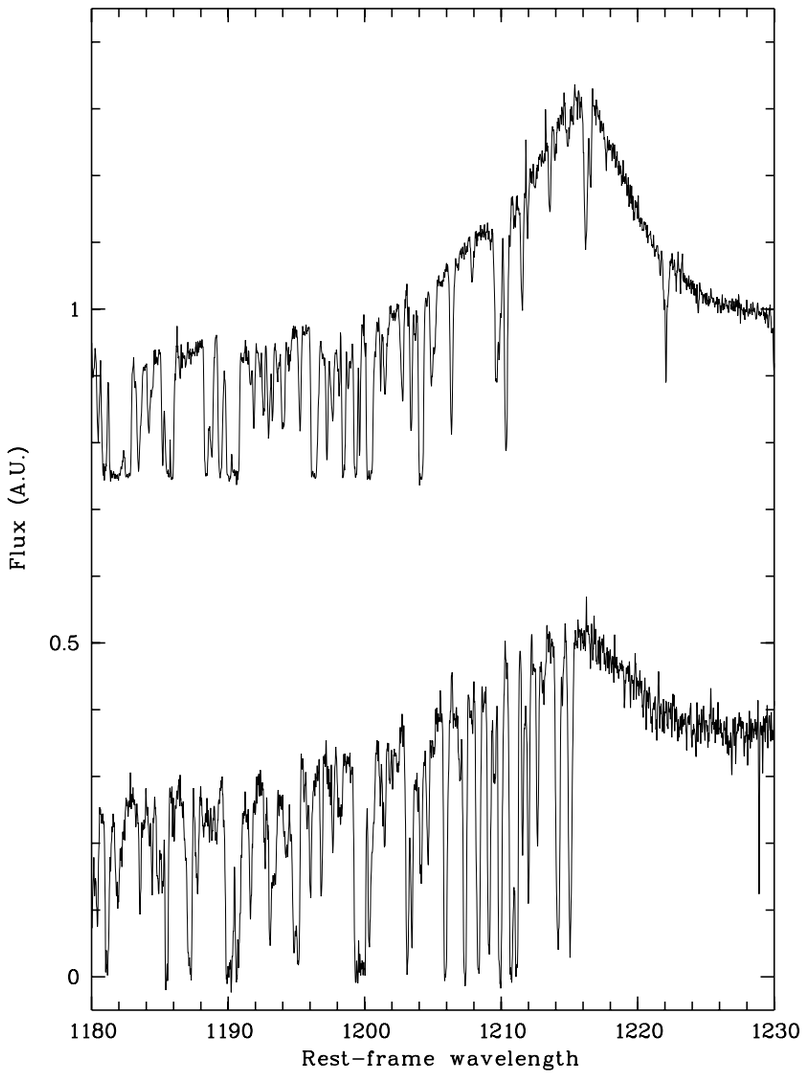

Giallongo, Fontana, Cristiani, D'Odorico 1999

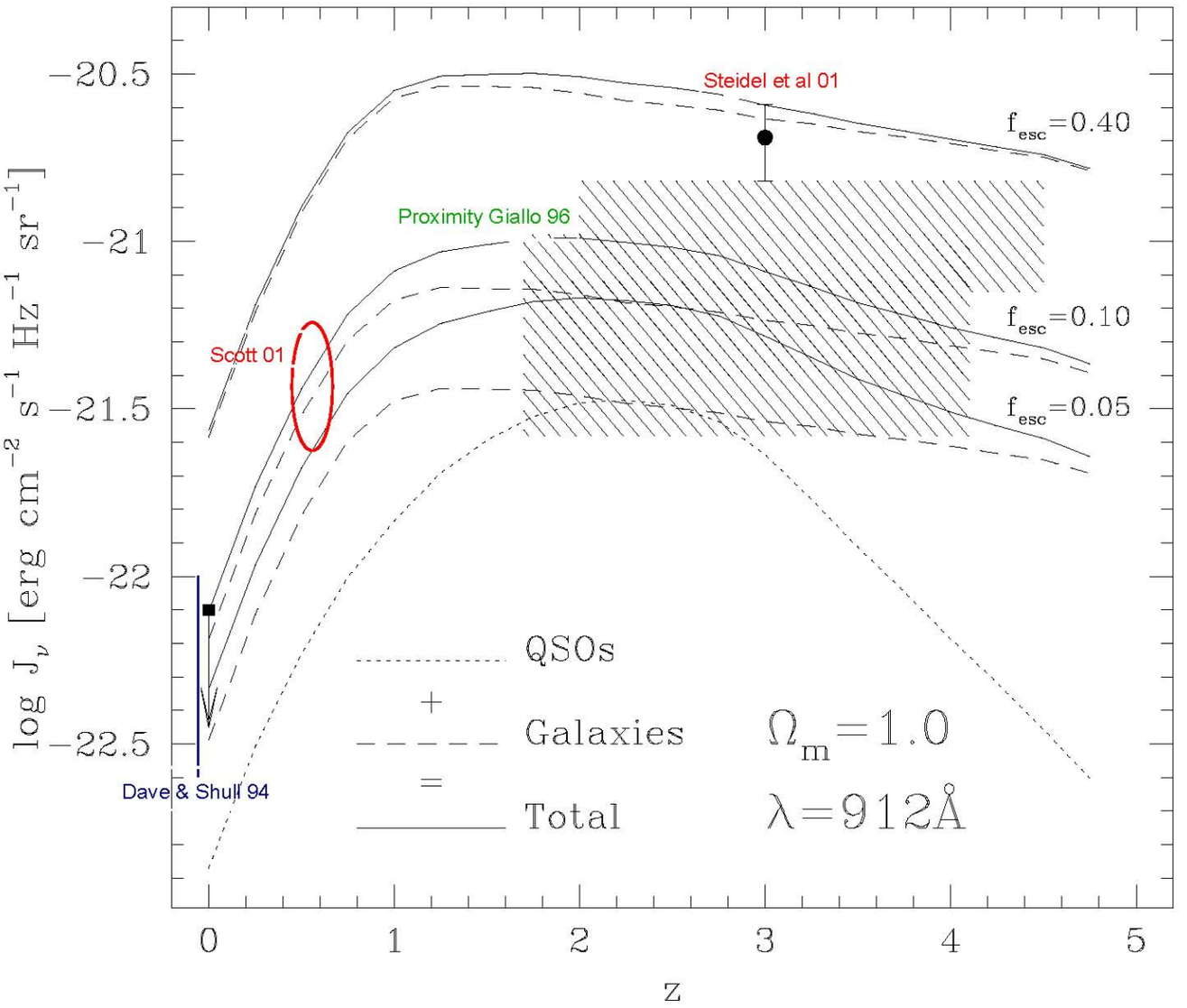

Bianchi S., Cristiani, Kim 2001

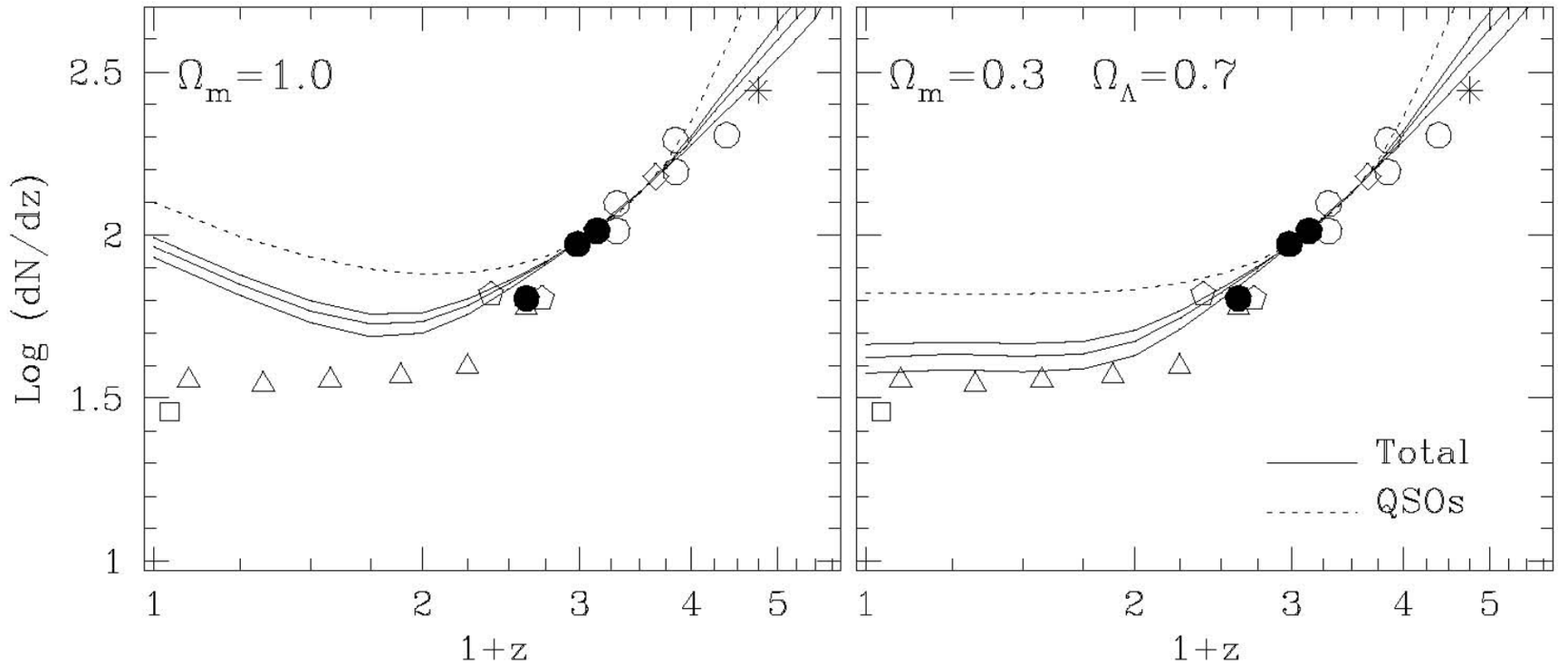

Bianchi S., Cristiani, Kim 2001

•A galaxy contribution to the UV BKG corresponding to $f_{esc} \simeq 0.05-0.1$ is sufficient to improve the agreement of the predictions with the observed $\aleph(z)$

•$\Omega_\Lambda = 0.7, \Omega_m = 0.3$ describe the $\aleph(z)$ better than $\Omega_m = 1$

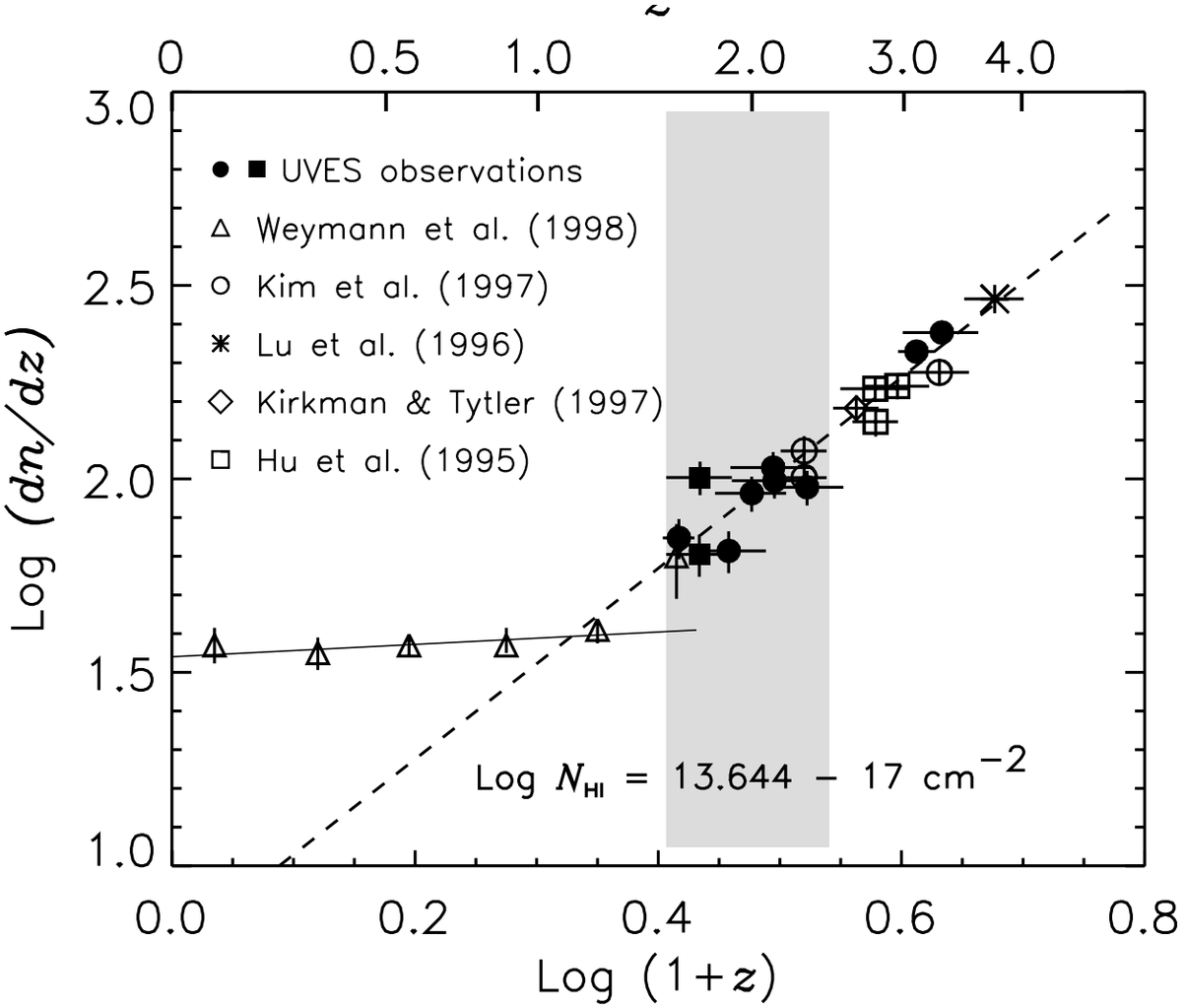

$$N(z) = N_o\,(1+z)^{\gamma} = 6.5\,(1+z)^{2.3\pm0.2} \qquad (5)$$

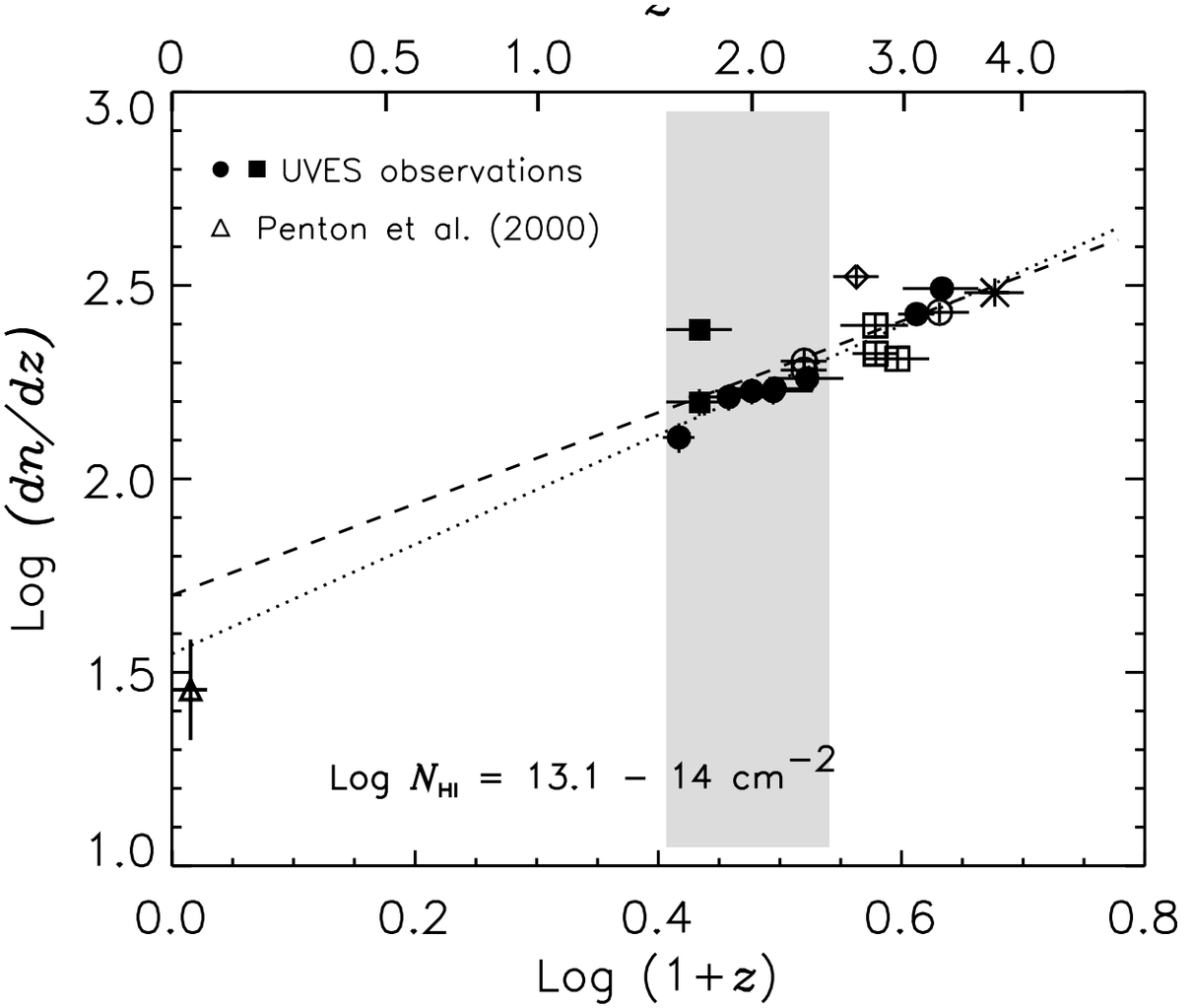

$$N(z) = N_o\,(1+z)^{\gamma} \qquad \gamma \simeq 1.3 \qquad (6)$$